batteries

MDPI

Review

Advances in Vanadium-Redoxed Polyanions for High-Voltage Sodium-Ion Batteries

Honglun Wu [1], Yiqing Chen [1], Tianzhuo Wen [1], Long Chen [1], Xiangjun Pu [2,*] and Zhongxue Chen [1,*]

[1] School of Power and Mechanical Engineering, Wuhan University, Wuhan 430072, China
[2] Department of Industrial and Systems Engineering, The Hong Kong Polytechnic University, Hung Hom, Hong Kong 999077, China
* Correspondence: xiangjun.pu@polyu.edu.hk (X.P.); zxchen_pmc@whu.edu.cn (Z.C.)

Abstract: Large-scale energy storage using sodium ion batteries (SIBs) as a hub for the conversion of renewable energy has become a topic of great importance. However, the application of SIBs is hindered by low energy density arising from inferior capacity and operation voltage. In this regard, vanadium-based phosphate polyanions with multiple valence changes (III–V), high redox potential, abundant resources, spacious frame structure, and remarkable thermal stability are promising avenues to address this dilemma. In this review, following the principle of electronic structure and function relationship, we summarize the recent progress in phosphates, pyrophosphates, fluorophosphates, and mixed polyanions of vanadium-centered polyanionic materials for SIBs. This review may provide comprehensive understanding and guidelines to further construct high performance, low-cost sodium-ion batteries.

Keywords: high-voltage; V-based polyanions; sodium-ion batteries

check for updates

Citation: Wu, H.; Chen, Y.; Wen, T.; Chen, L.; Pu, X.; Chen, Z. Advances in Vanadium-Redoxed Polyanions for High-Voltage Sodium-Ion Batteries. *Batteries* **2023**, *9*, 56. https://doi.org/10.3390/batteries9010056

Academic Editor: Catia Arbizzani

Received: 9 November 2022
Revised: 8 January 2023
Accepted: 10 January 2023
Published: 12 January 2023

1. Introduction

In recent years, as the price of lithium resources has rapidly grown, sodium ion batteries (SIBs) have become more competitive in the field of large-scale electrochemical energy storage (EES) [1,2]. Sodium is abundant in the Earth's crust and in sea water, and is thus more available than lithium (element concentrations in the upper continental crust: Li = 22 ppm, Na = 25,670 ppm) [3]. As shown in Figure 1a, the working principle of SIBs is similar to that of lithium-ion batteries (LIBs) [4]. However, SIBs have been plagued by low theoretical capacity and sluggish insertion/extraction kinetics, owing to the larger ionic radius and greater atomic mass of Na^+ [5]. Considering that large-scale EES demands higher power density to conduct frequent peak regulation, SIBs have encountered challenges with respect to their practical application [6]. Cathode materials are also an essential aspect of the electrochemical performance and reliability of SIBs. Their inherent crystal structure determines essential attributes such as electron transfer number, redox potential, and the charge-transfer kinetics.

There are four primary kinds of cathode materials for SIBs: Prussian blue, transition metal oxides, organic compounds, and polyanionic compounds. The comparison of these four types of compounds is displayed in Figure 1b. Generally, Prussian blue ($A_xM[Fe(CN)_6]_y \cdot zH_2O$) has an open framework structure and good structural stability [7,8]. However, the crystal water in the structure results in large amounts of $Fe(CN)_6$ vacancies, largely restricting the material's electrochemical properties. Transition metal oxides possess a high specific capacity and a moderate working voltage, but are also limited by the structural changes and phase transitions that occur during electrochemical processes and by inferior air stability [9]. Organic compounds have also been considered as potential cathodes for SIBs owing to their structural diversity, micro-regulatory properties, and resource sustainability, but their widespread application has been limited by their low intrinsic electronic conductivity and low operating voltage [10]. Compared with these

other candidates, polyanionic compounds possess a comprehensive manifestation of relatively high operating voltage, specific energy (vs. Na^+/Na), operation reliability, and safety [11–13].

Among polyanionic compounds, vanadium (V)-based polyanionic compounds have tended to receive more attention in recent years due to their many merits [14]. On one hand, V has a higher abundance in the upper continental crust as compared to Co, Ni, Cu, and Cr, making it more available (Figure 1c) [3]. On the other hand, vanadium possesses a valence electron configuration of $3d^3 4s^2$, which allows it to experience a multivalent electrochemical reaction from V^{3+} to V^{5+}. Additionally, many V-based polyanionic compounds exhibit a high operating voltage of over 3.4 V (vs. Na^+/Na) owing to the inductive effect of polyanionic groups and V redox (see Table 1). A schematic diagram of inductive effects is presented in Figure 1d [15]. When the M–O bond is more covalent, the antibonding orbitals will be pushed up, resulting in larger energy splitting between antibonding and bonding orbitals, as well as lower redox potential. As shown in Figure 1e, with a similar theoretical capacity of ~97 mAh g^{-1}, a higher operating voltage remarkably increases the theoretical specific energy (vs. Na^+/Na). When another atom X with stronger electronegativity is introduced to form M–O–X bonds, the inductive effect begins to take effect since the covalency between M–O will be lowered, leading to higher voltage [16]. Hence, the redox voltage can be effectively improved by introducing different polyanionic groups in cathode materials. In addition, the unique open framework often endows V-based polyanionic compounds with outstanding cycle stability and rate performance [4].

To date, several reviews of polyanionic compounds have been conducted with respect to their classification, crystal structures, and common electrochemical performance [4,14,17–19]. Nevertheless, to the best of our knowledge, there has not been a unique summary and interpretation of the high voltage properties of V-based polyanionic compounds, although this type of material is an essential candidate for SIBs. For a simple sample, and to have a comprehensive comparison of typical cathode materials for SIBs, we included their voltages and specific energies (vs. Na^+/Na) in Figure 1f [4,7,8]. As can be seen, V-based polyanionic compounds have a moderate specific energy (vs. Na^+/Na) but a relatively high voltage; thus, a systematic interpretation is necessary to build better a understanding of the causes, effects, and strategies for further enhancing V-based electrodes.

In this review, we will concentrate on high-voltage V-based polyanionic compounds ($\geq$3.4 V) and present a comprehensive interpretation in terms of their structure, charge transfer kinetics, Na^+ storage mechanisms, and electrochemical performance. In addition, modification approaches, major defects, challenges, and perspectives on the application of V-based electrode materials for SIBs will be also presented.

Table 1. A comparison of V-based polyanionic compounds as cathode materials for SIBs.

Materials	Structure	Redox (V)	Redox Couple	Theoretical Capacity (mAh g^{-1})	Theoretical Specific Energy (vs. Na^+/Na) (Wh kg^{-1})	Electrochemical Activity
$Na_3V_2(PO_4)_3$ [21,22]	Rhombohedral	3.4	V^{4+}/V^{3+}	117.6	400	117 mAh g^{-1} at 1 C 82 mAh g^{-1} at 100 C
$Na_3V_3(PO_4)_4$ [23]	Monoclinic (layered structure)	3.9	V^{4+}/V^{3+}	44.5	174	~40 mAh g^{-1} at 0.6 C
$Na_3V(PO_4)_2$ [24]	Monoclinic (layered structure)	3.5	V^{4+}/V^{3+}	90	315	~90 mAh g^{-1} at 0.2 C
$VOPO_4$ [25]	Tetragonal (layered structure)	3.4	V^{5+}/V^{4+}	165.5	563	150 mAh g^{-1} at 0.05 C
$NaVOPO_4$ [26]	Monoclinic	3.6	V^{5+}/V^{4+}	145	522	101 mAh g^{-1} at 5 mA g^{-1}
$NaVOPO_4$ [27]	Orthorhombic	3.3	V^{5+}/V^{4+}	145	479	115 mAh g^{-1} at 0.1 C
$NaVOPO_4$ [28]	Triclinic	3.5	V^{5+}/V^{4+}	145	508	144 mAh g^{-1} at 0.05 C
$Na_4VO(PO_4)_2$ [29,30]	Orthorhombic	3.5	V^{5+}/V^{4+}	78	273	41.3 mAh g^{-1} at 10 C

Table 1. *Cont.*

Materials	Structure	Redox (V)	Redox Couple	Theoretical Capacity (mAh g^{-1})	Theoretical Specific Energy (vs. Na^+/Na) (Wh kg^{-1})	Electrochemical Activity
$NaVPO_4F$ [31]	Tetragonal (NASICON)	3.7	V^{4+}/V^{3+}	142.5	527	120.9 mAh g^{-1} at 0.05 C 70.1 mAh g^{-1} at 0.5 C
$NaVPO_4F$ [32–34]	Monoclinic (NASICON)	3.4	V^{4+}/V^{3+}	142.5	484.5	135 mAh g^{-1} at 0.2 C 86.5 mAh g^{-1} at 100 C
$Na_5V(PO_4)_2F_2$ [35]	Trigonal/Orthorhombic	3.4/3.5	V^{4+}/V^{3+}	68	231.2/238	61 mAh g^{-1} at 0.1C
$Na_3V_2(PO_4)_2F_3$ [36,37]	Tetragonal (NASICON)	3.9	V^{4+}/V^{3+}	128.3	500	125 mAh g^{-1} at 0.2 C
$Na_3V_2(PO_4)_2O_2F$ [38,39]	Tetragonal	3.8	V^{5+}/V^{4+}	130	494	127.4 mAh g^{-1} at 0.2C
$Na_3V_2(PO_4)_2O_{1.6}F_{1.4}$ [40,41]	Tetragonal	3.8	V^{5+}/V^{4+}	129.7	492.9	134 mAh g^{-1} at 0.1 C
$NaVP_2O_7$ [42]	Monoclinic	3.9	V^{4+}/V^{3+}	108.1	421	104 mAh g^{-1} at 0.1 C
$Na_7V_3(P_2O_7)_4$ [43,44]	Monoclinic	4.13	V^{4+}/V^{3+}	79.6	329	67.2 mAh g^{-1} at 8 C
$Na_2VOP_2O_7$ [45]	Tetragonal	3.8	V^{5+}/V^{4+}	93.4	355	80 mAh g^{-1} at 0.05 C
$Na_7V_4(P_2O_7)_4(PO_4)$ [46,47]	Tetragonal	3.85	V^{4+}/V^{3+}	92.7	357	92 mAh g^{-1} at 0.05 C 70.2 mAh g^{-1} at 10 C
$Na_2(VO)_2(HPO_4)_2(C_2O_4)$ [48]	Monoclinic	4.0	V^{5+}/V^{4+}	116.6	466.4	105 mA h g^{-1} at 0.1 C

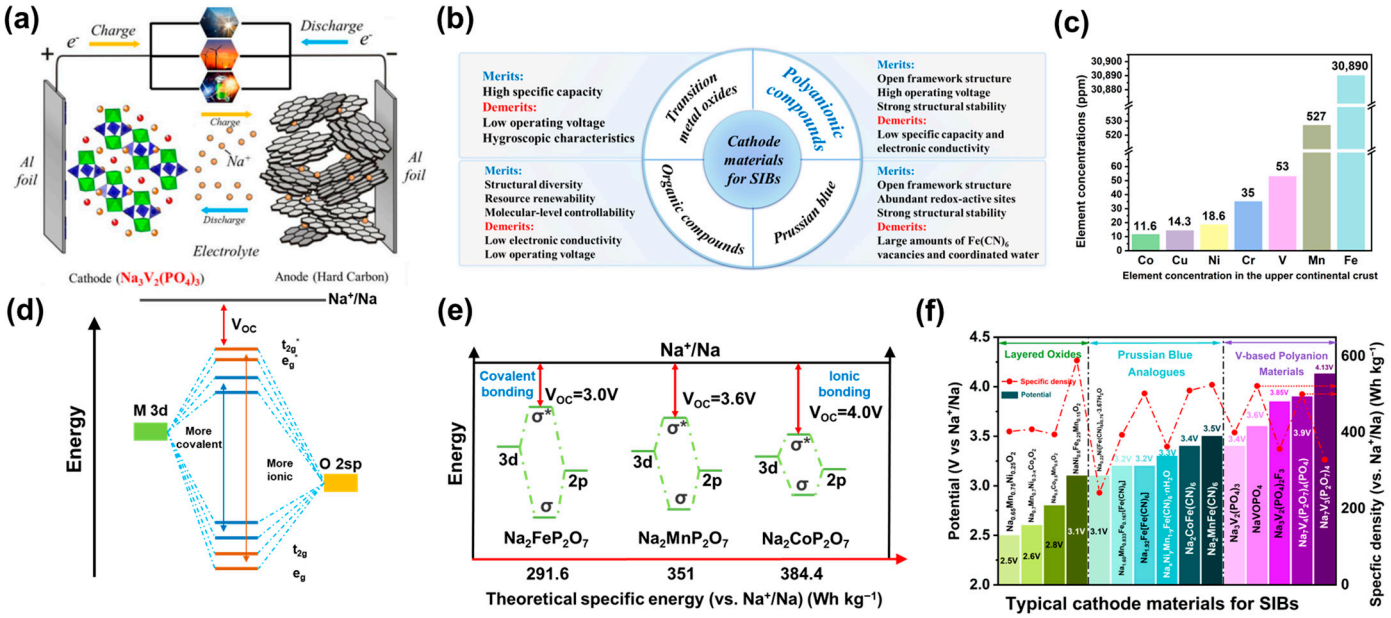

Figure 1. (**a**) Working principle of room-temperature SIBs [20]. (**b**) Comparison of various cathode materials for SIBs [20]. (**c**) Element concentrations of Co, Cu, Ni, Cr, V, Mn, and Fe (in ppm) in the upper continental crust [3]. (**d**) Schematic diagram of the influence of the M-O bond on the orbital energy level and operating potential (*Voc*). (**e**) Schematic illustration showing the relationship of *Voc* and theoretical specific energy (vs. Na^+/Na). (**f**) Potential and specific energies (vs. Na^+/Na) of typical cathode materials for SIBs.

2. Phosphate

V-based phosphates have been widely investigated owing to their high operating potential, and outstanding thermal and structural stability. The inductive effect of the $(PO_4)^{3-}$ polyanion endows them with high potential, while the strong P–O bond ensures a stable structure during the charge–discharge process. To date, numerous compounds including $Na_3V_2(PO_4)_3$, $Na_3V_3(PO_4)_4$, VOPO4, $NaVOPO_4$, and $Na_4VO(PO_4)_2$ have been confirmed to have high operation potential.

2.1. $Na_3V_2(PO_4)_3$ (3.4 V vs. Na^+/Na, the Same Hereinafter)

The well-known $Na_3V_2(PO_4)_3$ (NVP) has the rhombohedral NASICON structure with the space group $R\bar{3}c$ [49,50]. Figure 2a shows its 3D structure; the isolated VO_6

octahedra and PO_4 tetrahedra are connected to form the framework $[V_2(PO_4)_3]^{3-}$ along the c direction. The unit cell of $Na_3V_2(PO_4)_3$ is constructed of six formula units and two kinds of Na^+ sites with different coordination environments, which are referred to as the Na1 site and Na2 site. The structure can provide spacious diffusion paths to ensure sodium ions' intercalation/deintercalation in the structure [50]. Meanwhile, two different types of Na^+ occupy two oxidation state channels in the lattice, namely the Na1 site and the Na2 site. The skeleton structure is prone to be stable during the extraction of two Na^+ ions because of the tightly bonded covalent influence of $(PO_4)_3$. Figure 2b displays the galvanostatic cycling profile within the voltage range of 2.3–3.9 V for a $Na_3V_2(PO_4)_3$/C electrode [51]. With a flat plateau at 3.4 V vs. Na^+/Na, two Na^+ ions can be released from the host material to form $NaV_2(PO_4)_3$, resulting in a high theoretical capacity of 117.6 mAh g^{-1} [20]. During the charge/discharge process, a highly reversible bi-phase reaction based on V^{3+}/V^{4+} has been observed [52]. When charge from $Na_3V_2(PO_4)_3$ to form $NaV_2(PO_4)_3$, calculations using density functional theory (DFT) have indicated that Na^+ prefers to diffuse through the inside Na layers, such that Na^+ ions located at the Na1 site tend to remain while the rest of the Na^+ ions at the Na2 site can be extracted [53,54].

To optimize the performance of high-voltage NVP, several types of modification strategies have been tested to address the poor intrinsic conductivity of $Na_3V_2(PO_4)_3$, including carbon coating, nano crystallization, and ionic doping. Carbon coating has been widely used to promote the electronic conductivity of electrode materials. Generally, construction of a carbon layer and conductive agents can enhance electronic conductivity, and thus the electrochemical performance of electrode materials [52,55,56]. Additionally, heteroatom doping (N, S, P, B, etc.) can also cause carbon layers by defects [57–60]. Nano crystallization of the cathode materials can increase the specific surface area and decrease ions' diffusion paths [61–63]. Although carbon coating and nano crystallization are efficient approaches to improve electrochemical performance, they cannot change the inherent characteristics of a material. Hence, tests of anionic doping (Ti^{4+}, Fe^{3+}, Li^+, Mn^{2+}, Cr^{2+}) and anionic ions (F^-, Cl^-) have been conducted to specifically modify the deep electrons' structure. To enhance the voltage, Zakharkin et al. selected Mn^{2+} to partially replace V^{3+} and successfully synthesized $Na_{3+x}Mn_xV_{2-x}$ $(PO_4)_3$ ($0 \leq x \leq 1$) samples [57]. An additional high-voltage plateau (~3.9 V) was found in all Mn-substituted samples and $Na_{3+x}Mn_xV_{2-x}(PO_4)_3$ (x = 0.4) exhibited 8–10% additional specific energy (vs. Na^+/Na) in comparison to bare $Na_3V_2(PO_4)_3$ (Figure 2c). Further phase transformations in the voltage window of 2.5–3.8 V were also investigated, and it was found that several single- and two-phase actions exist during Na^+ (de)intercalation (Figure 2d), thus leaving more opportunities for novel composition. For anionic ions, Chen et al. synthesized F-doped $Na_3V_2(PO_4)_3$/C composites [58]. The modified $Na_3V_2(PO_4)_{2.93}F_{0.07}$/C presented a higher electronic conductivity and better cycle performance (86% retention after 1000 cycles at 200 mA g^{-1}).

2.2. $Na_3V_3(PO_4)_4$ (3.9 V)

Recently, a novel 3.9 V layered $Na_3V_3(PO_4)_4$ was explored as a potential cathode material for SIBs. It is isostructural with $Na_3Fe_3(PO_4)_4$ (ICSD No. 95532) with space group C2/*c* [23]. As shown in Figure 2e, due to the inductive effect, nearly one Na^+ ion can be extracted from the structure of $Na_3V_3(PO_4)_4$ with a high voltage plateau at 3.9 V, which is the highest V^{3+}/V^{4+} couple among V-based phosphates. From the perspective of thermodynamics, DFT calculations have also confirmed the high theoretical potential of 4.03 V when the first Na atom is removed from the original unit cell. However, it exhibited a low discharge capacity of 34 mAh g^{-1} and further exploration is still necessary.

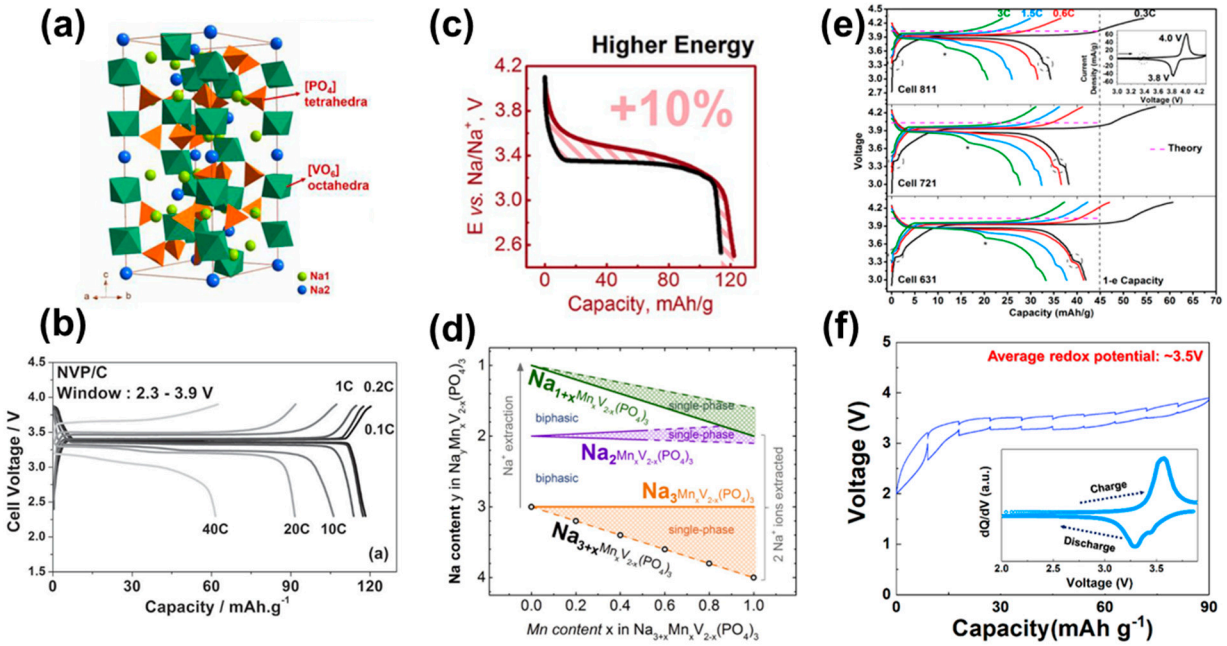

Figure 2. (**a**) Crystal structure of $Na_3V_2(PO_4)_3$ [50]. (**b**) Charge/discharge curves of $Na_3V_2(PO_4)_3$/C at various current rates in the voltage range 2.3–3.9 V [51]. (**c**) Improvement of the specific energy (vs. Na^+/Na) for Mn-doped $Na_3V_2(PO_4)_3$. (**d**) Schematic diagram of the Na^+ deintercalation mechanism for $Na_{3+x}Mn_xV_{2-x}(PO_4)_3$ ($0 \leq x \leq 1$) during Na^+ extraction [57]. (**e**) Charge/discharge curves of $Na_3V_3(PO_4)_4$ at different current densities between 3.0–4.3 V. Inset is the relative CV profile at 0.05 mV s^{-1} [23]. (**f**) The quasi-open-circuit potential profile of $Na_3V(PO_4)_2$ tested at C/20 and calculated average voltage. Inset is the dQ/dV profiles of $Na_3V(PO_4)_2$ [24].

2.3. $Na_3V(PO_4)_2$ (3.5 V)

Another ratio in this derivative is the peculiar $Na_3V(PO_4)_2$, which is identical to the structure of $Na_3Fe(PO_4)_2$ in the monoclinic (C2/*c*) space group [24,64]. It has a layered structure, consisting of VO_6 octahedra and PO_4 tetrahedra. As shown in Figure 2f, a flat voltage plateau at ~3.5 V (vs. Na^+/Na) can be observed in quasi-open-circuit potential and dQ/dV profiles. During Na (de)intercalation, it experiences a biphasic reaction between $Na_3V(PO_4)_2$ and $Na_2V(PO_4)_2$ with only one Na able to be exacted form the structure, leading to a theoretical capacity of 90 mAh g^{-1}, even when charged to 4.2 V [65,66]. To address this drawback, Liu et al. attempted to extend the upper cut-off voltage to 4.3 V [67]. ^{51}V solid-state NMR was employed to confirm that the high-voltage plateau can be attributed to V^{4+}/V^{5+} reactions. Therefore, $Na_3V(PO_4)_2$ has the potential to deliver two electrons through $V^{3+}/V^{4+}/V^{5+}$ reactions with a higher theoretical specific energy (vs. Na^+/Na) of 657 Wh kg^{-1}. However, the poor reversibility of V^{4+}/V^{5+} severely influences the cycle performance, calling for more work to tackle this this dilemma.

2.4. $VOPO_4$ (3.4 V)

Besides Na–V orthophosphates with different element ratios, vanadyl orthophosphates are enriching the high-voltage family. Prior to its application to SIBs in the last decade, $VOPO_4$ had already been recognized as a potential cathode material in LIBs owing to its high operating voltage and specific capacity. There are several types of crystal structures for $VOPO_4$ in terms of layered α_1, α_2, δ, ω, and γ, as well as three-dimensional β and ε phases, and all of them are composed of independent PO_4 tetrahedra sharing vertices with VO_6 octahedra, but they differ with respect to the orientation of the vanadyl bond [68,69]. He et al. first prepared layered $VOPO_4$ via chemical delithiation of the tetragonal α_1-$LiVOPO_4$, delivering a reversible capacity of 110 mAh g^{-1} at 0.05 C with an obvious potential plateau at 3.4~3.5 V (Figure 3a) [25]. Additionally, introducing highly conductive reduced graphene

oxide (rGO) can significantly increase the specific capacity of α_1-$VOPO_4$ to 150 mAh g^{-1}, amounting to 0.9 Na^+ per formula. Yu et al. synthesized tetragonal $VOPO_4$ to achieve a high-rate capability of 70 mAh g^{-1} at 5 C, as well as 136 mAh g^{-1} at 0.1 C [70]. Further, a $Na_2Ti_3O_7$/$VOPO_4$ full cell was tested by Yu's group [71]. The full cell presented a high operating voltage (~2.9 V) and reversible capacity (114 mAh g^{-1} at 0.1C and 74 mAh g^{-1} at 2 C) with a high specific energy (vs. Na^+/Na) of 220 Wh kg^{-1}. Very recently, Zhang et al. found that $VOPO_4$•$2H_2O$ can fulfill consecutive V^{5+}/V^{4+}/V^{3+} redox reactions [72]. Abundant phases bring more possibilities but also troubles for synthesis, thus preparing the targeted phase without side products is a major challenge for $VOPO_4$.

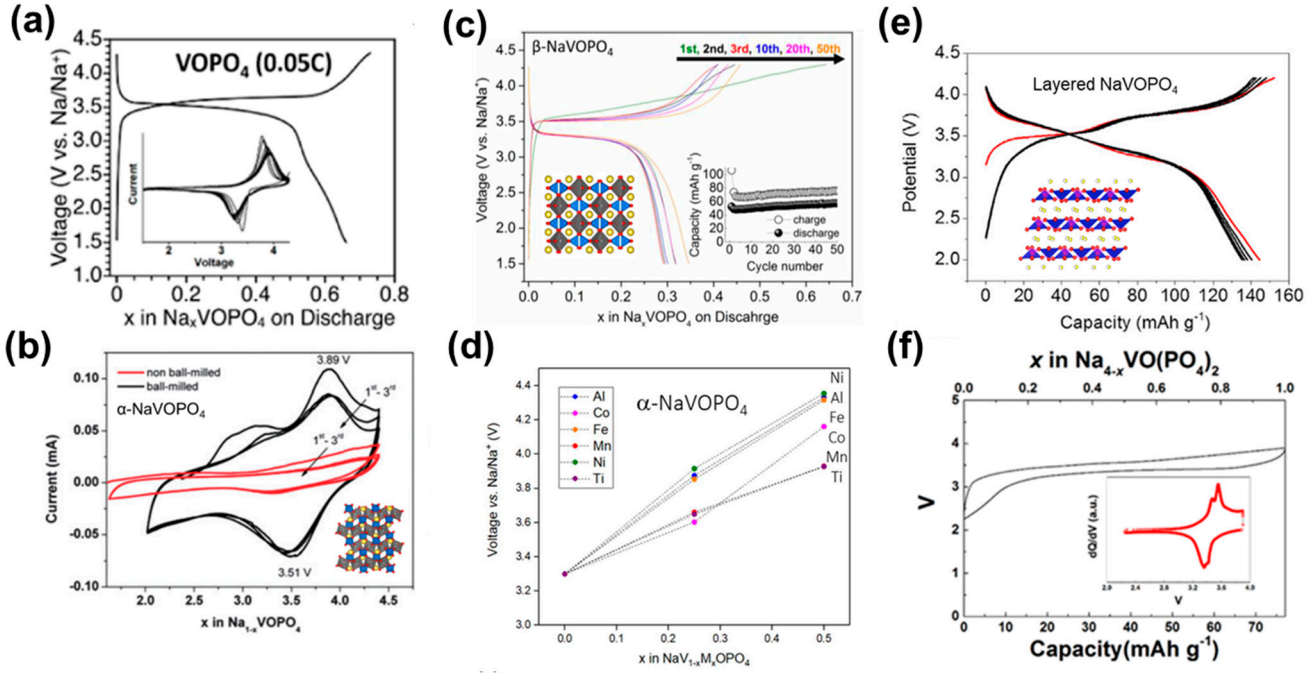

Figure 3. (**a**) Typical charge–discharge curves and CV (inset) between 1.5–4.3 V of the layered $VOPO_4$ electrodes [25]. (**b**) CV profiles (scan rate at 0.1 mV s^{-1}) and crystal structure of α-$NaVOPO_4$ [73]. (**c**) Charge–discharge curves of β-$VOPO_4$ at C/20 (8 mA g^{-1}) between 4.3 and 1.5 V. Insets show the crystal structure and cycling capacities [74]. (**d**) How the type and concentration of dopants on the V site influence the cell voltage (vs. Na^+/Na) in the α-$NaVOPO_4$ polymorphs (M = Al^{3+}, Co^{2+}, Fe^{3+}, Mn^{4+}, Ni^{2+}, or Ti^{4+}) [75]. (**e**) Lattice structure and galvanostatic charge–discharge profiles of the layered $NaVOPO_4$ electrode at a current rate of 0.05 C (1 C = 145 mA g^{-1}) [28]. (**f**) Charge/discharge curve of $Na_4VO(PO_4)_2$. Inset is dQ/dV [29].

2.5. $NaVOPO_4$ (3.3 V/3.5 V/3.6 V Due to Phase Difference)

Na-deficient $VOPO_4$ needs to be pre-sodiated to become a Na-rich cathode for Na-ion battery applications, causing it to be quite costly, time consuming, and complex; however, $NaVOPO_4$ containing reasonable amounts of Na has been studied as well. Similar to $VOPO_4$, $NaVOPO_4$ also has abundant phase states, such as monoclinic lattice α (space group: P21/*c*), tetragonal lattice α_1 (space group: P4/nmm), orthorhombic lattice β (space group: Pnma), and layered structured $NaVOPO_4$. α-$NaVOPO_4$ was first explored as a cathode material for SIBs by Goodenough et al. [73]. As shown in Figure 3b, with an average potential of 3.6 V (vs. Na^+/Na), it exhibits a reversible capacity of 90 mAh g^{-1} at 1/15 C. As shown in Figure 3c, β-$NaVOPO_4$ possesses a moderate potential plateau at 3.3 V and a high theoretical capacity of 145 mAh g^{-1} based on a V^{5+}/V^{4+} redox couple [27,74]. However, its actual capacity was greatly affected by the invasion of protons into the structure, leading to large irreversible capacity. α_1-$NaVOPO_4$ was built up of $VOPO_4$ sheets stacked along the c axis to show a typical layered structure. Na^+ ions are adequately accommodated in the space between two $VOPO_4$ planes because of the large interlayer spacing. On the basis

of molecular dynamics simulations, it has been found to have the highest Na^+ mobility among the α, β, and α_1 polymorphs [75]. DFT+U was also employed to investigate the influence of cell voltage on the $NaVOPO_4$ polymorphs when doping on the vanadium site. As shown in Figure 3d, the promotion of cell voltage is tend to occur with cation doping (Al^{3+}, Fe^{3+}, Mn^{4+}, Co^{2+}, Ni^{2+}, and Ti^{4+}) at the vanadium site. Fang et al. prepared another layered $NaVOPO_4$ with a triclinic lattice (Figure 3e) [28]. It attains a high voltage of ~3.5 V (vs. Na^+/Na) and a high discharge capacity of 144 mAh g^{-1} at 0.05 C. Besides these crystals, an amorphous $NaVOPO_4$ was reported to exhibit high reversible capacity (110 mAh g^{-1} at 0.05 C) at ~3.5 V (vs. Na^+/Na), as well as a capacity retention of 96% after 2000 cycles, showing an outstanding cyclability [76]. Additionally, some derivatives of $NaVOPO_4$ have also been shown to be feasible hosts for Na ions. For instance, based on a multi-electron transfer with V^{3+}/V^{5+} redox reactions, $KVOPO_4$ could exhibit an extremely high specific capacity of 235 mAh g^{-1} at 2.56 V, which can be attributed to its unique polyhedral framework [77].

2.6. $Na_4VO(PO_4)_2$ (3.5 V)

$Na_4VO(PO_4)_2$, indexed into a space group of orthorhombic *Pbca*, is the Na sufficient member of V-based oxygenous phosphates [30]. As can be seen from the charge/discharge profile and the dQ/dV presented in Figure 3f, one Na ion in $Na_4VO(PO_4)_2$ can be reversibly (de)intercalated from the structure with an average voltage of ~3.5 V (vs. Na^+/Na) and a theoretical capacity of 78 mAh g^{-1} [29]. Based on the V^{4+}/V^{5+} redox reaction, the reaction mechanism turns out to be a one-phase reaction. Additionally, Deriouche et al. also examined the electrochemical performance of the $Na_4VO(PO_4)_2$ compound, and found that is has high ionic conductivity and stability up to 700 °C [78]. Recently, DFT calculations and molecular dynamics simulations were employed to further study the electronic structure and influence of cation doping for $Na_4VO(PO_4)_2$ [30]. The results indicated a diffusion coefficient of D_{Na} = 5.1*10^{-11} cm^2 s^{-1} at 300 K and a Na ion activation energy of 0.49 eV. Additionally, the cell voltage is also predicted to increase by cation doping at the vanadium site. Nevertheless, similar to the prediction of $NaVOPO_4$, the practical performance of cation doping should be confirmed by experiment.

In short, V-based phosphates have excellent durability and fast kinetics, which can be attributed to their open channel structure and compositional stability. However, the operation voltage is still limited due to the inherent nature of PO_4, limiting the feasibility of its introduction into other groups with strong inductive effect.

3. Fluorophosphate and Vanadyl Fluorophosphate

Fluorine substitution for phosphate groups is possible to promote the operating voltage because of the stronger inductive effect of F^-. To date, several F-containing V-based polyanionic compounds, including $NaVPO_4F$, $Na_5V(PO_4)_2F_2$, $Na_3V_2(PO_4)_2F_3$, and $Na_3V_2O_{2x}(PO_4)_2F_{3-2x}$ have been investigated as high voltage cathodes for SIBs.

3.1. $NaVPO_4F$ (3.7 V)

Compared with the other members of V-based polyanionic compounds, $NaVPO_4F$ has a higher theoretical specific capacity of 143 mAh g^{-1} (compare 117 mAh g^{-1} for $Na_3V_2(PO_4)_3$ and 128 mAh g^{-1} for $Na_3V_2(PO_4)_2F_3$), making it a promising choice for SIBs. Currently, research shows that $NaVPO_4F$ can exist in two phases: a tetragonal symmetric structure with space group I4/mmm, and a monoclinic structure with space group C2/c [79]. The tetragonal phase is isostructural with $Na_3Al_2(PO_4)_2F_3$ while the monoclinic phase presents an analogous structure to $NaAlPO_4F$ (ICSD no. 040522) (Figure 4a) [80,81]. Even with exactly the same chemical composition, the sodium storage properties of the two compounds vary greatly. The tetragonal $NaVPO_4F$ possesses a theoretical capacity of 143 mAh g^{-1} based on a V^{4+}/V^{3+} redox reaction at 3.7 V. The monoclinic $NaVPO_4F$ shows a relatively low working plateau of 3.4 V with a single-phase reaction (Figure 4b) [32,34]. Further reports found that the tetragonal $NaVPO_4F$ tends to experience an irreversible tran-

sition to the monoclinic phase when the sintering temperature reaches up to ~750 °C, due to lower formation energy (i.e., more stable nature) of monoclinic $NaVPO_4F$ as compared to the tetragonal phase (Figure 4a) [79,82]. Additionally, after surface coating and structure modification, the monoclinic phase seems to have capacity and rate merits compared to the other phase [83,84].

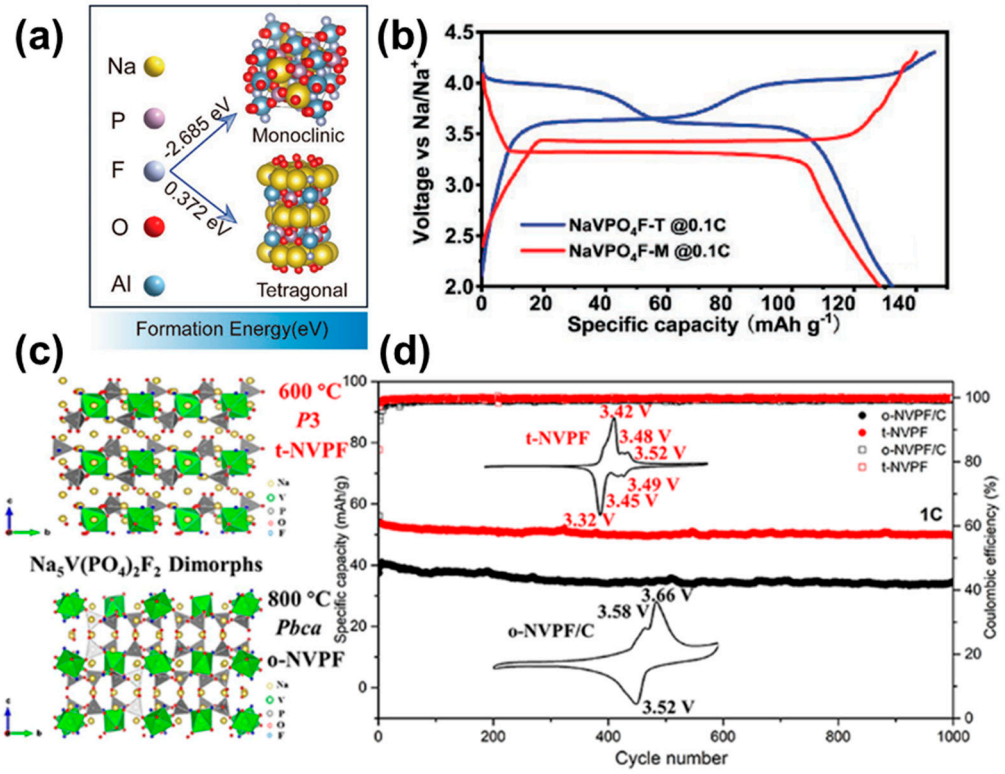

Figure 4. (**a**) The formation energy calculated by DFT methods and (**b**) galvanostatic charge/discharge curves at 0.1C of $NaVPO_4F$-M and $NaVPO_4F$-T [79]. (**c**) The crystal structure and (**d**) cyclability, as well as CV curves, of o-$Na_5V(PO_4)_2F_2$/C and t-$Na_5V(PO_4)_2F_2$ [35].

In short, the tetragonal phase is more suitable as a high-energy-density cathode, mainly due to strong ionic bonding, while the monoclinic crystal is feasible for high power applications due to the intrinsically faster charge transfer kinetics.

3.2. $Na_5V(PO_4)_2F_2$ (3.4 V/3.5 V)

Layered $Na_5V(PO_4)_2F_2$ has recently been investigated as a potential cathode material for SIBs, owing to its high voltage and good cycling stability. Interestingly, as shown in Figure 4c, it has two types of structures depending on the calcination temperatures. Under high temperatures, reaching 800 °C, the obtained phase turns out to be identical with the orthorhombic $Na_5Fe(PO_4)_2F_2$ (PDF 87-1031) with a space group *P3*, which is referred as o-$Na_5V(PO_4)_2F_2$. The other phase, t-$Na_5V(PO_4)_2F_2$, is isostructural to the trigonal $Na_5Cr(PO_4)_2F_2$ (PDF 77-0506), indexed into space group *Pbca*, and can be formed at a relatively low temperature of 600 °C [35]. Due to the different sodium coordinative environments in the two phases, Na^+ ions in t-$Na_5V(PO_4)_2F_2$ are more likely to migrate along the *c* axis, while they prefer to migrate along the ac plane in o-$Na_5V(PO_4)_2F_2$. The material presents an operating voltage of 3.4 V for trigonal-type and 3.5 V for orthorhombic-type, based on the V^{3+}/V^{4+} redox couple (Figure 4d). During the charging process, a biphasic process followed by a monophasic process was confirmed by ex situ XRD and DFT calculations for both phases. However, only one Na ion can be reversibly extracted/inserted, resulting in a poor specific capacity of ~62 mAh g^{-1} at 0.1C (1C = 136 mA g^{-1}). Further reports have indicated that higher sodium ion activation barriers and possible structural

decomposition of the intermediate phase make it difficult to remove two sodium ions from $Na_5V(PO_4)_2F_2$ [85].

3.3. $Na_3V_2(PO_4)_2F_3$ (3.9 V)

Among V-based fluorophosphate, $Na_3V_2(PO_4)_2F_3$ displays the highest working voltage (~3.9 V vs. Na^+/Na) due to the strong ionicity of the F–V bond, and high specific energy (vs. Na^+/Na).

$Na_3V_2(PO_4)_2F_3$ has a tetragonal symmetry structure with a space group of P42/*mnm*, and is composed of $[V_2O_8F_3]$ bi-octahedral units and $[PO_4]$ tetrahedral units connected by shared O atoms (Figure 5a) [86]. This arrangement generates channels along the *a* and *b* directions with sodium located in the tunnel sites, providing apparent pathways for diffusion of Na ions [87,88]. $Na_3V_2(PO_4)_2F_3$ delivers a theoretical capacity of 128 mAh g^{-1} with two potential plateaus at 3.7 V and 4.2 V, based on a two-step redox reaction of V^{3+}/V^{4+} (Figure 5b) [86]. Two different environments for Na ions resulted in respective Na (de)insertion, which generated a difference of 0.4–0.5 V between the two voltage plateaus. Although the high working voltage (about 3.9 V), large theoretical capacity, and fast ionic mobility enables $Na_3V_2(PO_4)_2F_3$ to be a promising cathode material for SIBs, the poor intrinsic electronic conductivity often leads to high inner resistance, low coulombic efficiency, and limited rate performance, which seriously affects its applications.

Many approaches have been employed to enhance the electronic conductivity of $Na_3V_2(PO_4)_2F_3$, such as heteroatom-doping [89], carbon-coating [90], morphology design [91,92], etc. In order to explore the possibility of modifying the values of the redox couples, anionic substitution of oxygen for fluorine has also been conducted. Hence, several vanadyl fluorophosphates including $Na_3V_2(PO_4)_2O_2F$ and $Na_3V_2(PO_4)_2O_{1.6}F_{1.4}$ have been further investigated.

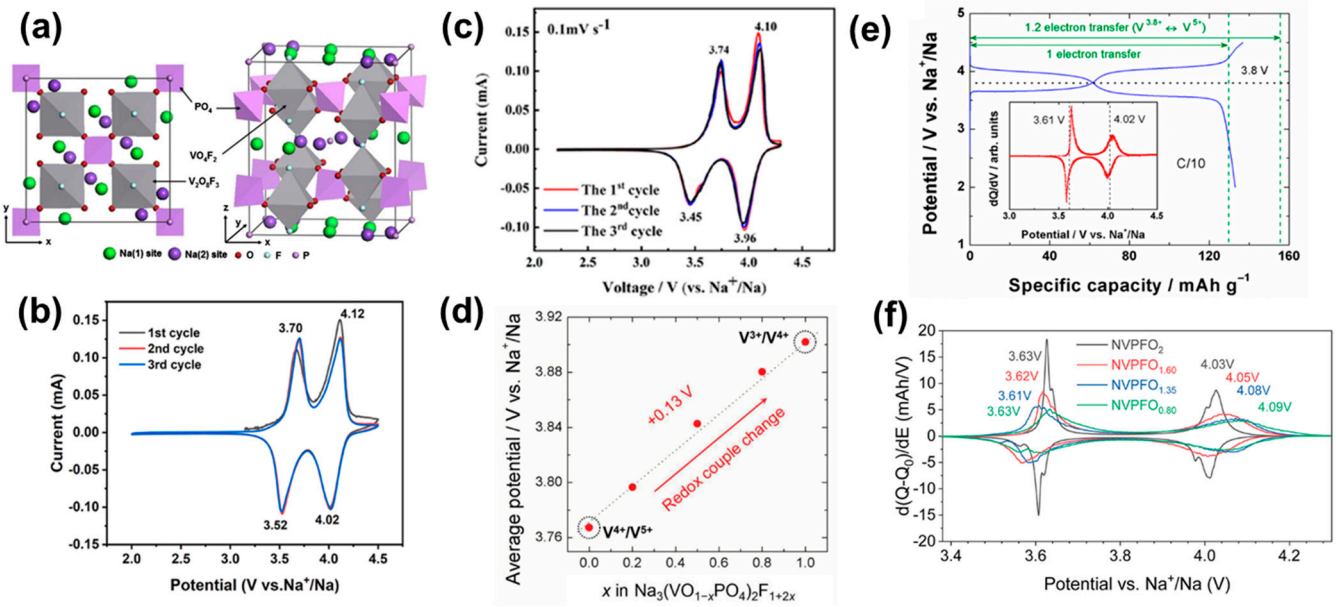

Figure 5. (**a**) The crystal structure of $Na_3V_2(PO_4)_2F_3$ [86]. (**b**) CV curves of $Na_3V_2(PO_4)_2F_3$ for the first three cycles at 0.1 mV s^{-1} [93]. (**c**) CV curves of $Na_3V_2(PO_4)_2O_2F$ at a scan rate of 0.5 mV s^{-1} [94]. (**d**) Tends in average voltages of the $Na_y(VO_{1-x}PO_4)_2F_{1+2x}$ compound as x increases. [95]. (**e**) Charge/discharge profile at a C/10 rate for the $Na_3V_2(PO_4)_2O_{1.6}F_{1.4}$ cathode and the corresponding dQ/dV curve inset [40]. (**f**) The dQ/dV curves for $Na_3V^{3+}{}_{2-y}V^{4+}{}_yO_y(PO_4)_2F_{3-y}$ electrode materials corresponding to the 5th cycle performed at C/20 [96].

3.4. $Na_3V_2O_{2x}(PO_4)_2F_{3-2x}$ ($0 < x \leq 1$)

$Na_3V_2(PO_4)_2F_3$ is actually the special member for x = 0 of a series of isostructural $Na_3V_2O_{2x}(PO_4)_2F_{3-2x}$ ($0 \leq x \leq 1$) compounds, the latter of which has three-dimensional $O_8F_{3-2x}O_{2x}$ bi-octahedral units linked together by phosphate groups via oxygen atoms, with the highly mobile Na ions present at the tunnel sites [97]. In spite of their similar crystal framework, the redox mechanism and phase reactions significantly deviate with the composition due to variations in covalent and ionic bonding, as we stated in the introduction section. $Na_3V_2O_{2x}(PO_4)_2F_{3-2x}$ ($0 < x < 1$) exhibits a slightly lower operating voltage than $Na_3V_2(PO_4)_2F_3$, because of the weaker electronegativity of O than of F [98]. Fortunately, they present a high theoretical capacity due to the extra Na^+ insertion/extraction below 4.5 V, since partial substitution of O for F can reduce the Na^+–Na^+ repulsion, thus allowing more Na to be accommodated. Here, two typical compounds in the series, $Na_3V_2(PO_4)_2O_2F$ and $Na_3V_2(PO_4)_2O_{1.6}F_{1.4}$, are discussed in detail.

3.4.1. $Na_3V_2(PO_4)_2O_2F$ (3.8 V)

When x = 1, the formula turns out to be $Na_3V_2(PO_4)_2O_2F$. It has a tetragonal symmetry within the I4/*mnm* space group [99]. Its crystal structure is constructed by layers of alternating [PO_4] tetrahedra and [VO_5F] octahedra. The layers in the structure are loosely interconnected over the F atoms along the *c* direction, forming a 3D open framework [100]. Two types of Na^+ sites were found: Na1 sites coordinated by one F atom and six O atoms, and Na2 sites coordinated six O atoms. As shown in Figure 5c, the reversible extraction of two Na^+ ions at voltages of ~3.6 and ~4.0 V (vs. Na^+/Na) in $Na_3V_2(PO_4)_2O_2F$ resulted in a theoretical capacity of 130 mA h g^{-1} and a theoretical specific energy (vs. Na^+/Na) of 486 Wh kg^{-1} [94]. As for the Na^+ storage mechanism, different hypotheses have been proposed based on characterizations. Based on an in situ XRD test, one typical statement indicates that the $Na_3V_2(PO_4)_2O_2F$ experiences two completely reversible biphasic transitions from $Na_3V_2(PO_4)_2O_2F$ to $Na_2V_2(PO_4)_2O_2F$, and then to $NaV_2(PO_4)_2O_2F$, as well as a low volumetric change during the charging and discharging processes [101]. Based on time-resolved in situ SXRD, another statement indicates a complex asymmetrical reaction during the Na^+ insertion/extraction process [102].

Similar to $Na_3V_2(PO_4)_2F_3$, the sluggish Na^+ diffusion kinetics and poor electronic conductivity of $Na_3V_2(PO_4)_2O_2F$ cause a rapid fading of capacity during Na^+ insertion/extraction and low specific energy (vs. Na^+/Na). Therefore, multiple surfaces, morphology, and crystal structure modification strategies have been developed to address the problems [38,103–105]. Investigation on the family of $Na_3(VO_{1-x}PO_4)_2F_{1+2x}$ ($0 \leq x \leq 1$) has been conducted to evaluate their performance. As shown in the Figure 5d, when x = 0 (or 1), the reaction between the charge/discharge process is only based on the V^{3+}/V^{4+} (or V^{4+}/V^{5+}) redox couple [95]. Owing to the strong inductive effect of F^- in fluorine-rich samples, the V^{3+}/V^{4+} redox potential of the latter (~3.9 V) was higher by ~0.13 V as compared to the V^{4+}/V^{5+} redox potential of the former (~3.77 V). The linear change in voltage may help us achieve a balance between voltage and capacity for higher specific energies (vs. Na^+/Na) via changing the x.

3.4.2. $Na_3V_2(PO_4)_2O_{1.6}F_{1.4}$ (3.8 V)

When x = 0.8, the formula turns out to be $Na_3V_2(PO_4)_2O_{1.6}F_{1.4}$. It is isostructural to both $Na_3V_2(PO_4)_2O_2F$ and $Na_3V_2(PO_4)_2F_3$ with a space group of $P4_2/mnm$ [41]. Benefiting from the open framework, $Na_3V_2(PO_4)_2O_{1.6}F_{1.4}$ possesses a theoretical capacity of 129.7 mAh g^{-1} based on one electron transfer with two potential plateaus at 3.61 and 4.02 V (vs. Na^+/Na). However, it can actually exhibit a higher reversible capacity of 134 mAh g^{-1} due to more electron transfer (Figure 5e) [40]. During the charge/discharge process, $Na_3V_2(PO_4)_2O_{1.6}F_{1.4}$ experiences a typical two-step solid-solution reaction while both V^{4+}/V^{5+} and V^{3+}/V^{4+} redox couples are active. Moreover, solid-state nuclear magnetic resonance and electron paramagnetic resonance have been employed to give a comprehensive understanding of the Na^+ extraction/intercalation process [106]. The results indicated that

V^{3+} mostly reacts in the high-potential charge region while V^{4+} continually translates to V^{5+} during the whole charge process. The influence of O content has also been investigated, and it was found that $Na_3V_2(PO_4)_2O_{1.6}F_{1.4}$ has broad and less defined peaks (Figure 5f) because of the solid solution reaction [96]. Meanwhile, the results indicated that the average redox potential of the second pseudo-plateau tends to rise with of the increase in fluorine content, which can be attributed to the more ionic V–F bond in comparison to the V=O one. Additionally, a small volume change (2.9%; $0.88 \leq x \leq 3$) upon cycling was observed, which guarantees a remarkable cycling stability and rate performance. For instance, a nanostructured $Na_3V_2(PO_4)_2O_{1.6}F_{1.4}$ exhibited, via microwave-assisted solvothermal procedure, excellent rate capability (67.2 mAh g^{-1} under 30 C) and long-term cycle performance (61 mAh g^{-1} after 1000 cycles at 10 C) when tested as a cathode for Na-ion coin cells [107].

Compared with $Na_3V_2(PO_4)_3$, V-based fluorophosphates present an elevated specific capacity and an improved potential, which can be attributed to the lighter molecular mass and stronger inductive effect of F^-. However, fluorine loss during heat treatment is a challenge, as fluorine is unstable in V-based fluorophosphates, and thus calls for proper preparation methods to precisely regulate material composition.

4. Pyrophosphates

Compared with phosphates and fluorophosphates, V-based pyrophosphates possess abundant crystal chemistry, robust structure, and superior Na^+ mobility, manifesting potential in application. To date, $NaVP_2O_7$, $Na_7V_3(P_2O_7)_4$, and $Na_2(VO)P_2O_7$ are typical representatives.

4.1. $NaVP_2O_7$ (3.9 V)

$NaVP_2O_7$ presents a relatively high operating voltage of 3.9 V and a theoretical capacity of 108.4 mAh g^{-1} [108,109]. As shown in Figure 6a, it has two types of crystal structures: α- and β-phase. α-$NaVP_2O_7$ is isostructural with the monoclinic $NaMoP_2O_7$, delivering a poor reversible capacity of 40 mAh g^{-1} [42]. β-$NaVP_2O_7$ isotypic to the monoclinic $KAlP_2O_7$, and could be operated at 3.9 V vs. Na/Na^+ (Figure 6b) with a reversible capacity of 104 mAh g^{-1}. The different structures of the two phases leads to lower migration barrier in the β-phase and thus disparate electrochemical performances. The diffusion of Na in α-$NaVP_2O_7$ was slower by several orders of magnitude than that of β-$NaVP_2O_7$, making β-$NaVP_2O_7$ a more suitable cathode material than the α-phase. β-$NaVP_2O_7$ also exhibited good high-rate performance (77 mAh g^{-1} at 50 C) and low stable galvanostatic cycling with only 0.5% of volume change. Similar to $Na_2(VO)P_2O_7$, further research on $NaVP_2O_7$ is still limited.

4.2. $Na_7V_3(P_2O_7)_4$ (4.13 V)

Owing to the strong inductive effects of $P_2O_7^{4-}$, $Na_7V_3(P_2O_7)_4$ possesses the highest redox potential to date among reported vanadium-based cathode materials for SIBs. It is isotypic to the disordered form of $Na_7Fe_3(P_2O_7)_4$ (ICSD:86437), which can be indexed into a monoclinic space group of C2/*c* [110]. Previous studies have shown that $Na_7V_3(P_2O_7)_4$ exhibits a reversibility of ~80 mAh g^{-1} at an average voltage of 4.13 V (vs. Na^+/Na) based on the V^{3+}/V^{4+} redox couple (Figure 6c,d) [43]. Additionally, the electrode also presented a good rate capability with 75% initial capacity retention after 600 cycles at 1 C, which can be attributed to the open framework and low volume change (~1%) of the material during charge/discharge possess. Recently, detailed Na^+ extraction/insertion processes of $Na_7V_3(P_2O_7)_4$ have been investigated. As shown in Figure 6e, the charge capacity can be increased up to 106 mA h g^{-1} with extraction of about 4 Na^+ ions via activation of the V^{4+}/V^{5+} redox couple at higher voltages [44]. However, this Na^+ insertion/extraction reaction at high voltage is not fully reversible. In a wider voltage window of 1.3–4.8 V vs. Na^+/Na, operando X-ray diffraction was employed to determine the theoretical selective order of Na^+ extraction/insertion, demonstrating that the capacity of polyanionic materials may be promoted by the activation of additional redox couples for metal ions.

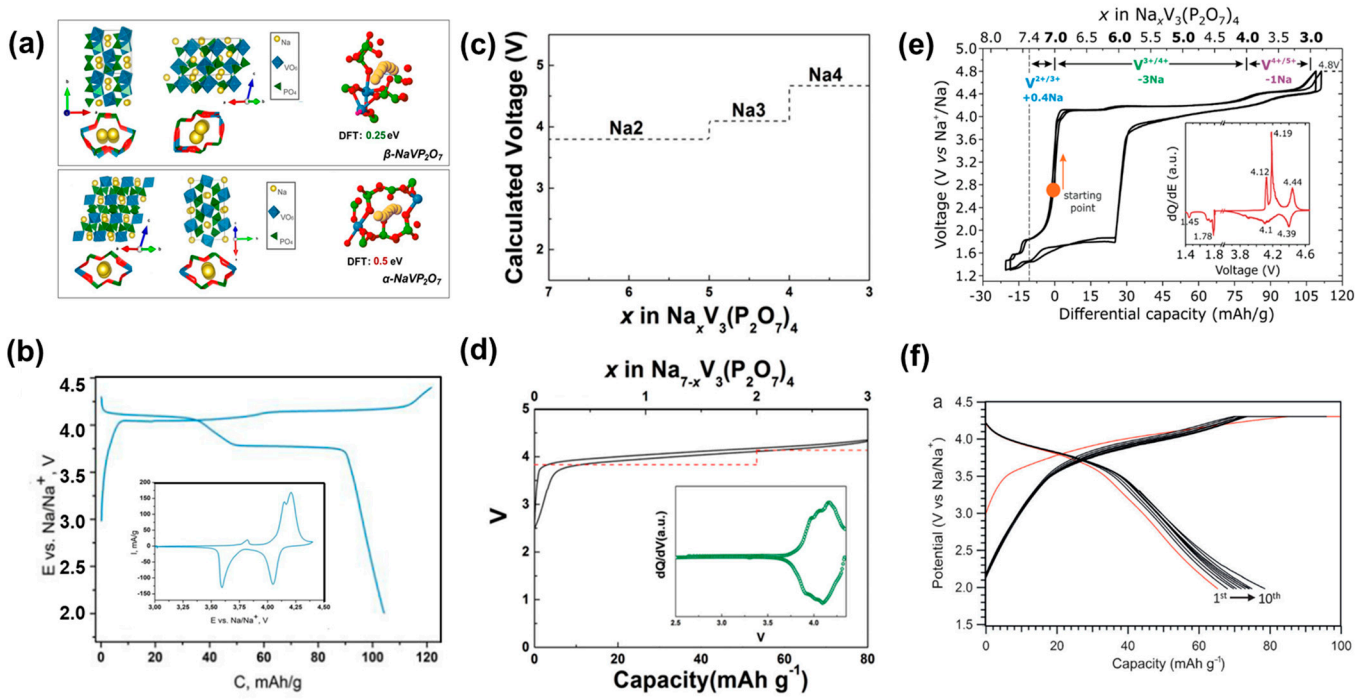

Figure 6. (**a**) The crystal structure, shortest Na^+ migration pathways, and migration barriers of β-$NaVP_2O_7$ and α-$NaVP_2O_7$. (**b**) Galvanostatic charge–discharge curves for β-$NaVP_2O_7$ collected at 10 mA g^{-1} current density between 2.0 and 4.4 V vs. Na^+/Na. Inset is the CV measurement for β-$NaVP_2O_7$ performed within 2.0–4.5 V [42]. (**c**) Calculation results of average redox potential for $Na_xV_3(P_2O_7)$. (**d**) Charge/discharge curves for $Na_7V_3(P_2O_7)_4$. Inset is the dQ/dV profile of $Na_7V_3(P_2O_7)_4$ [43]. (**e**) First two cycles of $Na_7V_3(P_2O_7)_4$ in the extended range of 1.3–4.8 V [44]. (**f**) Galvanostatic characterization of $Na_2(VO)P_2O_7$ cathode [45].

4.3. $Na_2(VO)P_2O_7$ (3.8 V)

Introducing vanadyl into pyrophosphates may be another promising approach. Dating back to 1998, tetragonal $Na_2(VO)P_2O_7$ has been reported to have an excellent ionic conductivity of 3.05×10^{-5} S cm^{-1}, rendering it a potential candidate for cathode applications [111]. However, it has only been explored as a potential cathode material for SIBs in the last decade. Slabs of $[VP_2O_8]_\infty$ are piled up along the *c* direction, intercepted by slabs of Na atoms, and thus a layered framework with Na atoms located along the tunnels is constructed. Moreover, the structure lets Na^+ preferentially diffuse between the layers, which can be considered a 1D conductor for Na diffusion. As can be seen in the charge/discharge curves displayed in Figure 6f, the $Na_2(VO)P_2O_7$ can deliver a reversible capacity of ~80 mAh g^{-1} at 3.8 V based on a V^{5+}/V^{4+} redox reaction, while its theoretical capacity is 93.4 mAh g^{-1} [45]. Different from $Na_7V_3(P_2O_7)_4$, the reaction of $Na_2(VO)P_2O_7$ is mainly based on the V^{5+}/V^{4+} redox couple rather than activating it for higher voltage.

Generally, pyrophosphates possess a relatively high operating voltage but a low specific capacity because of the strong inductive effect and large molecular mass of $P_2O_7^{4-}$. Additionally, low theoretical specific capacity and poor conductivity mainly limited their development. Therefore, partially (rather than completely) replacing PO_4 with $P_2O_7^{4-}$ and other polyanions to generate mixed polyanions may be an effectively way to handle this dilemma.

5. Mixed Polyanions

As mentioned above, by combining various polyanionic units, the concept of "mixed polyanionic compounds" has been proposed. This kind of combination can not only result in multiple electron redox activity and abundant structural diversity, but also regulate the redox voltage via different degrees of inductive effect. Among V-based mixed-polyanionic compounds, $Na_7V_4(P_2O_7)_4(PO_4)$ and $Na_2(VO)_2(HPO_4)_2(C_2O_4)$ are two typical representatives.

5.1. $Na_7V_4(P_2O_7)_4(PO_4)$ (3.85 V)

$Na_7V_4(P_2O_7)_4(PO_4)$ is indexed to a tetragonal structure (P-421c) in which a 3D open framework and well-defined ionic channels can serve for Na (de)insertion. Lim et al. reported that $Na_7V_4(P_2O_7)_4(PO_4)$ can exhibit an initial capacity of 91.0 mAh g^{-1} with a retention of ~78% over 1000 cycles [112]. The CV curve and charge/discharge profiles of $Na_7V_4(P_2O_7)_4(PO_4)$ are displayed in Figure 7a,b [46]. It exhibits a single-valued voltage plateau at 3.88 V vs. Na^+/Na based on the V^{3+}/V^{4+} redox reaction. Moreover, Deng et al. found the intermediate phase of $Na_5V^{3.5+}{}_4(P_2O_7)_4(PO_4)$ during the sodium de/intercalation of a $Na_7V_4(P_2O_7)_4(PO_4)$ nanorod [113]. As a result, the potential plateau can be subdivided into 3.87 V ($V^{3+}/V^{3.5+}$) and 3.89 V ($V^{3.5+}/V^{4+}$) (Figure 7c). Methods of carbon coating and structure have also been employed to improve the performance of $Na_7V_4(P_2O_7)_4(PO_4)$ [47,114–116]. Recently, an interesting study indicated that $Na_7V_4(P_2O_7)_4PO_4$ can be used for both cathode and anode materials owing to the operating voltage of 3.85 V and 0.94 V, respectively [46]. They assemble a symmetric full battery which exhibits an initial capacity of 81.9 mAh g^{-1} at 2.84 V. Although the compound possesses a high operating voltage and well-defined plateau, a relatively low capacity due to the heavy P_2O_7 group and the complexity still restricts its wide application.

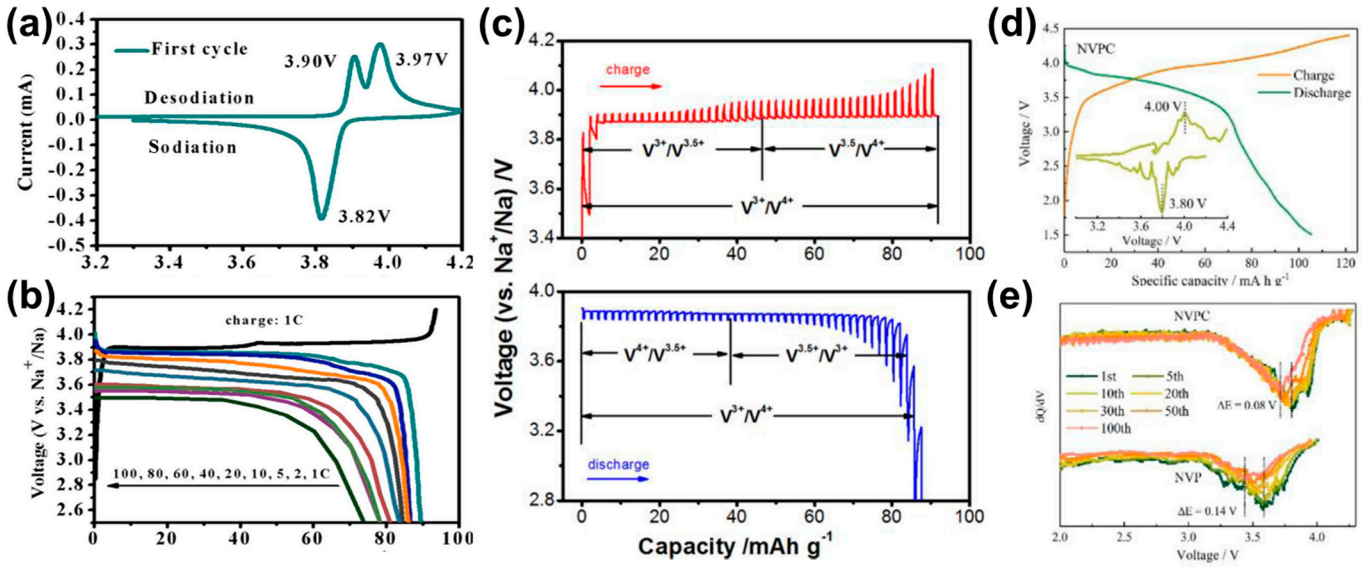

Figure 7. (**a**) CV curve at a scan rate of 0.1 mV s^{-1} in 3.3–4.2 V and (**b**) the charge/discharge curves at various rates of the $Na_7V_4(P_2O_7)_4(PO_4)$/C-GA cathode [46]. (**c**) The GITT charge and discharge curves of a $Na_7V_4(P_2O_7)_4(PO_4)$ nanorod [115]. (**d**) Galvanostatic charge/discharge curves and the corresponding dQ/dV patterns of $Na_2(VO)_2(HPO_4)_2(C_2O_4)$. (**e**) The dQ/dV plots of different cycles of $Na_2(VO)_2(HPO_4)_2(C_2O_4)$ and $Na_3V_2(PO_4)_3$ at 0.2 C [48].

5.2. $Na_2(VO)_2(HPO_4)_2C_2O_4$ (4.0 V)

Generally, the V^{5+}/V^{4+} redox reaction suffers from poor reversibility in other polyanionic compounds, leading to rapid capacity degradation. A solution is to employ the coupling of $(C_2O_4)^{2-}$ and $(HPO_4)^{2-}$ to result in a smaller forbidden band gap and lower energy barrier 2D Na^+ ion migration paths, as well as to stabilize reversible high-valent

redox of V^{4+}/V^{5+}. Very recently, Li et al. reported a V-based mixed-polyanion sodium oxalate-phosphate compound, formulated $Na_2(VO)_2(HPO_4)_2(C_2O_4)$ [48]. As shown in Figure 7d, it exhibited a high redox potential of 4.0/3.8 V and a considerable reversible capacity of 105.4 mAh g^{-1} based on the V^{4+}/V^{5+} redox couple. The high redox potential is confirmed by the dQ/dV plots (inset), which can be attributed to the accumulated inductive effect of mixed anions. As shown in Figure 7e, the corresponding dQ/dV curves of different cycles indicated the low voltage decay of only 0.08 V in the $Na_2(VO)_2(HPO_4)_2(C_2O_4)$ electrode. Hence, this showed the decent cycling stability with an initial capacity retention of 74.7% after 100 cycles at 0.2 C and 61.2% after 1000 cycles at 5 C.

The concept of mixed polyanions brings us new ideas regarding cathode materials. However, the complexity of the components limits the preparation methods and influences the phase purity; thus, to determine their electrochemical performance, more work is necessary to decipher this puzzle.

6. Summary and Perspectives

In this review, the structure, Na^+ storage mechanisms, charge transfer kinetics, and electrochemical performance of members among V-based polyanionic phosphates, fluorophosphates, vanadyl fluorophosphates, pyrophosphates, and mixed polyanions were systematically introduced and interpreted. A comprehensive comparison of their potential, specific capacity, and specific energy (vs. Na^+/Na) is displayed in Figure 8.

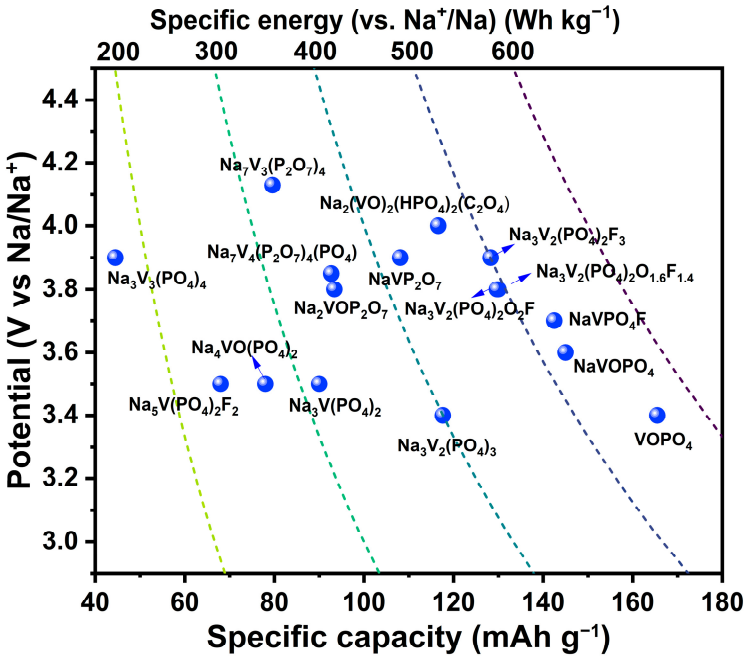

Figure 8. Comparisons among V-based polyanionic compounds for SIBs.

V-based phosphates have been widely investigated because of their high operating potential, and outstanding structural and thermal stability. The inductive effect of the $(PO_4)^{3-}$ polyanion endows them with high potential while the strong P–O bond ensures stable structure during charge–discharge process. However, they are short on efficient methods to further promote the working voltage, and the stronger inductive effect of F atoms made them a substitution alternative to further promote operating voltage. V-based fluorophosphates present a relatively higher operating voltage and specific capacity but also suffer from fluorine loss during heat treatment. Pyrophosphates possess rich crystal chemistry, stable structure, and superior Na^+ mobility, manifesting potential in application. However, the high molecular mass of $P_2O_7^{4-}$ leads to low theoretical specific capacity, although mixed polyanions seem to be a promising idea. Therefore, a balance of voltage

and capacity is likely to be achieved using mixed polyanions, but the complexity of the components limits the synthetic methods and their electrochemical performance. In short, V-based phosphates are the most promising cathode material for massive applications, while fluorophosphates have the potential to achieve higher operating voltage and specific energy (vs. Na^+/Na).

Although encouraging progress has been achieved in V-based polyanionic materials for SIBs, obstacles still remain that must be addressed. A comprehensive conclusion will help us to better understand the future of high-voltage V-based polyanionic materials:

1. Improvement in the operating voltage. Although V-based polyanionic compounds present relatively high operating voltages, more work is still urgently needed to further enhance the voltage of V^{n+1}/V^{n+} (n = 2,3,4) redox couples as well as specific energies (vs. Na^+/Na). There are three primary strategies to improve the operating voltage: utilization of inductive effect, activation of the V^{5+}/V^{4+} redox couple, and substitution of functional elements. On one hand, owing to the inductive effect, the stronger electronegativity of X and a more ionic M–O bond will always result in a higher working voltage for the M^{n+1}/M^{n+} redox couple. For the V^{3+}/V^{4+} redox couple, different groups exhibit diverse operating voltages, following the order of $P_2O_7 > PO_4F \approx (PO_4)_m(P_2O_7) > (PO_4)$. On the other hand, it is possible for V-based compounds are to exhibit a multi-electron reaction (involving V^{3+}/V^{2+}, V^{4+}/V^{3+}, and V^{5+}/V^{4+} redox couples). V^{4+}/V^{3+} is the most widespread redox couple with a moderate voltage, while an efficient way to achieve a much higher voltage is to activate the V^{5+}/V^{4+} redox couple at a higher voltage. Lastly, partially substituting vanadium with other high-voltage redox elements is also regarded as an efficient approach to promote voltage. Mn^{2+} and Co^{2+} may be ideal options and further investigation is necessary.
2. Developing new V-based polyanionic compounds. To achieve higher specific energy (vs. Na^+/Na), partially substituting heavy polyanionic groups (PO_4^{3-}, $P_2O_7^{4-}$) with other light groups (CO_3^{2-}, BO_3^{3-}, etc.) is a viable option. The oxalate–phosphate compound $Na_2(VO)_2(HPO_4)_2(C_2O_4)$ mentioned above is a referential instance. Additionally, considering the higher electronegativity for SO_4^{2-}, V-based sulfates may also an available way to achieve high-voltage material. Vanadium-based phosphate polyanionic compounds are competitive candidates for application in SIBs because of their high voltage, high power density, and cycle stability.
3. Although high-voltage V-based polyanionic compounds seem to be competitive candidate for SIBs, there is still a long way to go before their wide application (Figure 9). For instance, $Li_3V_2(PO_4)_3$ is a well-studied cathode material in Li-ion batteries but has not been commercialized for large-scale EES; however, the analysis of it may help us figure out the obstacles towards commercialization. $Li_3V_2(PO_4)_3$ provides a high capacity of 156.9 mAh g^{-1} within the voltage range of 3.0–4.8 V. However, its instability under high pressure, which may be caused by lithium–vanadium antisite mixing, necessitates researchers to limit the upper cut-off voltage to 4.3 V, resulting in uncompetitive specific energy (380 Wh kg^{-1} for $Li_3V_2(PO_4)_3$, ~496 Wh kg^{-1} for $LiFePO_4$, ~430 Wh kg^{-1} for $LiMn_2O_4$). In short, the performance gap with rival products makes it difficult to commercialize. Even if V-based compounds have comparative advantages over other transition metal compounds, challenges still remain before their mass production. First, while vanadium resources are abundant in the upper continental crust, the price of vanadium is higher when compared to Fe, etc. Additionally, the recycling of vanadium and vanadium dissolution are also urgent problems before commercialization. Lastly, the pollution and toxicity of vanadium have also been noteworthy issues. Research indicates that vanadium enrichment will become an ecological problem around vanadium-production areas. Meanwhile, vanadium is moderately toxic, and excess vanadium can cause certain damage to the body's organs and tissues. In general, if we can improve the production process of vanadium resources to reduce pollutants, and recycle V-based batteries at the end of

their life, then vanadium-based cathode materials will usher in a promising future and maintain exuberant vitality.

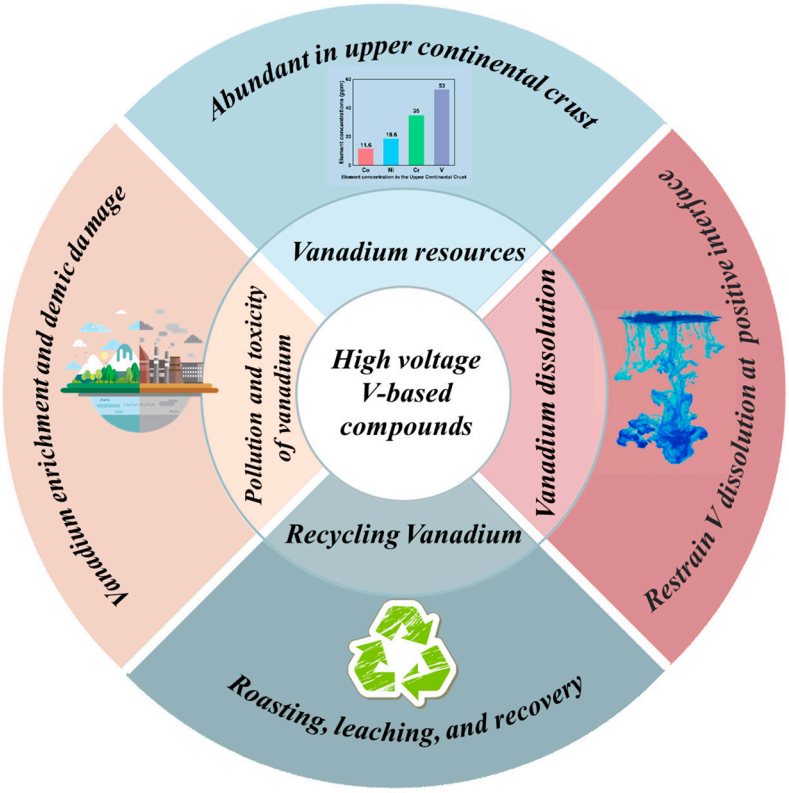

Figure 9. Perspective on the application of high-voltage V-based compounds [117].

Author Contributions: Conceptualization, X.P. and Z.C.; investigation, H.W. and Y.C.; data curation, H.W., T.W. and L.C.; writing—original draft preparation, H.W. and X.P.; writing—review and editing, H.W., X.P. and Z.C.; supervision, X.P. and Z.C.; funding acquisition, Z.C. All authors have read and agreed to the published version of the manuscript.

Funding: This work was financially supported by the National Natural Science Foundation of China (21875171 and U22A20438) and the Key R&D Plan of Hubei Province (2020BAA030).

Data Availability Statement: No data support.

Conflicts of Interest: The authors declare no conflict of interest.

References

1. Hu, Y.-S.; Lu, Y. 2019 Nobel Prize for the Li-Ion Batteries and New Opportunities and Challenges in Na-Ion Batteries. *ACS Energy Lett.* **2019**, *4*, 2689–2690. [CrossRef]
2. Liu, T.; Zhang, Y.; Jiang, Z.; Zeng, X.; Ji, J.; Li, Z.; Gao, X.; Sun, M.; Lin, Z.; Ling, M.; et al. Exploring competitive features of stationary sodium ion batteries for electrochemical energy storage. *Energy Environ. Sci.* **2019**, *12*, 1512–1533. [CrossRef]
3. Wedepohl, K.H. The composition of the continental crust. *Geochim. Cosmochim. Acta* **1995**, *59*, 1217–1232. [CrossRef]
4. Lv, Z.; Ling, M.; Yue, M.; Li, X.; Song, M.; Zheng, Q.; Zhang, H. Vanadium-based polyanionic compounds as cathode materials for sodium-ion batteries: Toward high-energy and high-power applications. *J. Energy Chem.* **2021**, *55*, 361–390. [CrossRef]
5. Khan, Z.; Vagin, M.; Crispin, X. Can Hybrid Na–Air Batteries Outperform Nonaqueous Na–O_2 Batteries? *Adv. Sci.* **2020**, *7*, 1902866. [CrossRef]
6. Pu, X.; Wang, H.; Zhao, D.; Yang, H.; Ai, X.; Cao, S.; Chen, Z.; Cao, Y. Recent Progress in Rechargeable Sodium-Ion Batteries: Toward High-Power Applications. *Small* **2019**, *15*, e1805427.
7. Song, J.; Wang, L.; Lu, Y.; Liu, J.; Guo, B.; Xiao, P.; Lee, J.; Yang, X.; Henkelman, G.; Goodenough, J. Removal of Interstitial H_2O in Hexacyanometallates for a Superior Cathode of a Sodium-Ion Battery. *J. Am. Chem. Soc.* **2015**, *137*, 2658–2664. [CrossRef]

8. Wu, X.; Wu, C.; Wei, C.; Hu, L.; Qian, J.; Cao, Y.; Ai, X.; Wang, J.; Yang, H. Highly Crystallized $Na_2CoFe(CN)_6$ with Suppressed Lattice Defects as Superior Cathode Material for Sodium-Ion Batteries. *ACS Appl. Mater. Interfaces* **2016**, *8*, 5393–5399. [CrossRef]
9. Sun, Y.; Guo, S.; Zhou, H. Adverse effects of interlayer-gliding in layered transition-metal oxides on electrochemical sodium-ion storage. *Energy Environ. Sci.* **2019**, *12*, 825–840. [CrossRef]
10. Yin, X.; Sarkar, S.; Shi, S.; Huang, Q.A.; Zhao, H.; Yan, L.; Zhao, Y.; Zhang, J. Recent Progress in Advanced Organic Electrode Materials for Sodium-Ion Batteries: Synthesis, Mechanisms, Challenges and Perspectives. *Adv. Funct. Mater.* **2020**, *30*, 908445.
11. Yuan, T.; Wang, Y.; Zhang, J.; Pu, X.; Ai, X.; Chen, Z.; Yang, H.; Cao, Y. 3D graphene decorated $Na_4Fe_3(PO_4)_2(P_2O_7)$ microspheres as low-cost and high-performance cathode materials for sodium-ion batteries. *Nano Energy* **2019**, *56*, 160–168. [CrossRef]
12. Pu, X.; Wang, H.; Yuan, T.; Cao, S.; Liu, S.; Xu, L.; Yang, H.; Ai, X.; Chen, Z.; Cao, Y. $Na_4Fe_3(PO_4)_2P_2O_7$/C nanospheres as low-cost, high-performance cathode material for sodium-ion batteries. *Energy Storage Mater.* **2019**, *22*, 330–336. [CrossRef]
13. Wang, H.; Pan, Z.; Zhang, H.; Dong, C.; Ding, Y.; Cao, Y.; Chen, Z. A Green and Scalable Synthesis of $Na_3Fe_2(PO_4)P_2O_7$/rGO Cathode for High-Rate and Long-Life Sodium-Ion Batteries. *Small Methods* **2021**, *5*, 2100372. [CrossRef] [PubMed]
14. Wang, Q.; Xu, J.; Zhang, W.; Mao, M.; Wei, Z.; Wang, L.; Cui, C.; Zhu, Y.; Ma, J. Research progress on vanadium-based cathode materials for sodium ion batteries. *J. Mater. Chem. A* **2018**, *6*, 8815–8838. [CrossRef]
15. Barpanda, P.; Lander, L.; Nishimura, S.-i.; Yamada, A. Polyanionic Insertion Materials for Sodium-Ion Batteries. *Adv. Energy Mater.* **2018**, *8*, 1703055. [CrossRef]
16. You, Y.; Manthiram, A. Progress in High-Voltage Cathode Materials for Rechargeable Sodium-Ion Batteries. *Adv. Energy Mater.* **2017**, *8*, 1701785. [CrossRef]
17. Fang, Y.; Chen, Z.; Xiao, L.; Ai, X.; Cao, Y.; Yang, H. Recent Progress in Iron-Based Electrode Materials for Grid-Scale Sodium-Ion Batteries. *Small* **2018**, *14*, 1703116. [CrossRef]
18. Jin, T.; Li, H.; Zhu, K.; Wang, P.F.; Liu, P.; Jiao, L. Polyanion-type cathode materials for sodium-ion batteries. *Chem. Soc. Rev.* **2020**, *49*, 2342–2377. [CrossRef]
19. Pan, W.; Guan, W.; Jiang, Y. Research Advances in Polyanion-Type Cathodes for Sodium-Ion Batteries. *Acta Phys. -Chim. Sin.* **2020**, *36*, 1905017.
20. Zheng, Q.; Yi, H.; Li, X.; Zhang, H. Progress and prospect for NASICON-type $Na_3V_2(PO_4)_3$ for electrochemical energy storage. *J. Energy Chem.* **2018**, *27*, 1597–1617. [CrossRef]
21. Zhang, J.; Zhao, X.; Song, Y.; Li, Q.; Liu, Y.; Chen, J.; Xing, X. Understanding the superior sodium-ion storage in a novel $Na_{3.5}Mn_{0.5}V_{1.5}(PO_4)_3$ cathode. *Energy Storage Mater.* **2019**, *23*, 25–34. [CrossRef]
22. Zhu, C.; Kopold, P.; van Aken, P.A.; Maier, J.; Yu, Y. High Power-High Energy Sodium Battery Based on Threefold Interpenetrating Network. *Adv. Mater.* **2016**, *28*, 2409–2416. [CrossRef]
23. Liu, R.; Liu, H.; Sheng, T.; Zheng, S.; Zhong, G.; Zheng, G.; Liang, Z.; Ortiz, G.F.; Zhao, W.; Mi, J.; et al. Novel 3.9 V Layered $Na_3V_3(PO_4)_4$ Cathode Material for Sodium Ion Batteries. *ACS Appl. Energy Mater.* **2018**, *1*, 3603–3606. [CrossRef]
24. Kim, J.; Yoon, G.; Kim, H.; Park, Y.-U.; Kang, K. $Na_3V(PO_4)_2$: A New Layered-Type Cathode Material with High Water Stability and Power Capability for Na-Ion Batteries. *Chem. Mater.* **2018**, *30*, 3683–3689. [CrossRef]
25. He, G.; Kan, W.H.; Manthiram, A. A 3.4 V Layered VOPO4 Cathode for Na-Ion Batteries. *Chem. Mater.* **2016**, *28*, 682–688. [CrossRef]
26. Chen, C.-Y.; Matsumoto, K.; Nohira, T.; Hagiwara, R. Improved Electrochemical Performance of $NaVOPO_4$ Positive Electrodes at Elevated Temperature in an Ionic Liquid Electrolyte. *J. Electrochem. Soc.* **2015**, *162*, A2093–A2098. [CrossRef]
27. Ni, Y.; He, G. Stable cycling of β-$VOPO_4$/$NaVOPO_4$ cathodes for sodium-ion batteries. *Electrochim. Acta* **2018**, *292*, 47–54. [CrossRef]
28. Fang, Y.; Liu, Q.; Xiao, L.; Rong, Y.; Liu, Y.; Chen, Z.; Ai, X.; Cao, Y.; Yang, H.; Xie, J.; et al. A Fully Sodiated $NaVOPO_4$ with Layered Structure for High-Voltage and Long-Lifespan Sodium-Ion Batteries. *Chem* **2018**, *4*, 1167–1180. [CrossRef]
29. Kim, J.; Kim, H.; Lee, S. High Power Cathode Material $Na_4VO(PO_4)_2$ with Open Framework for Na Ion Batteries. *Chem. Mater.* **2017**, *29*, 3363–3366. [CrossRef]
30. Aparicio, P.A.; de Leeuw, N.H. Electronic structure, ion diffusion and cation doping in the $Na_4VO(PO_4)_2$ compound as a cathode material for Na-ion batteries. *Phys. Chem. Chem. Phys.* **2020**, *22*, 6653–6659. [CrossRef]
31. Ruan, Y.-L.; Wang, K.; Song, S.-D.; Han, X.; Cheng, B.-W. Graphene modified sodium vanadium fluorophosphate as a high voltage cathode material for sodium ion batteries. *Electrochim. Acta* **2015**, *160*, 330–336. [CrossRef]
32. Ling, M.; Li, F.; Yi, H.; Li, X.; Hou, G.; Zheng, Q.; Zhang, H. Superior Na-storage performance of molten-state-blending-synthesized monoclinic $NaVPO_4F$ nanoplates for Na-ion batteries. *J. Mater. Chem. A* **2018**, *6*, 24201–24209. [CrossRef]
33. Cheng, B.; Zhang, S.; Zou, F.; Luo, L.; Chen, Y.; Chen, S.; Zhuo, H.; Zeng, X. Nano-$NaVPO_4F$ enwrapped in reduced graphene oxide as a cathode material for long-cycle and high-rate sodium-ion batteries. *J. Alloys Compd.* **2019**, *811*, 151828. [CrossRef]
34. Chen, C.; Li, T.; Tian, H.; Zou, Y.; Sun, J. Building highly stable and industrial $NaVPO_4F$/C as bipolar electrodes for high-rate symmetric rechargeable sodium-ion full batteries. *J. Mater. Chem. A* **2019**, *7*, 18451–18457. [CrossRef]
35. Liang, Z.; Zhang, X.; Liu, R.; Ortiz, G.F.; Zhong, G.; Xiang, Y.; Chen, S.; Mi, J.; Wu, S.; Yang, Y. New Dimorphs of $Na_5V(PO_4)_2F_2$ as an Ultrastable Cathode Material for Sodium-Ion Batteries. *ACS Appl. Energy Mater.* **2020**, *3*, 1181–1189. [CrossRef]
36. Wang, M.; Huang, X.; Wang, H.; Zhou, T.; Xie, H.; Ren, Y. Synthesis and electrochemical performances of $Na_3V_2(PO_4)_2F_3$/C composites as cathode materials for sodium ion batteries. *RSC Adv.* **2019**, *9*, 30628–30636. [CrossRef]

37. Yi, H.; Ling, M.; Xu, W.; Li, X.; Zheng, Q.; Zhang, H. VSC-doping and VSU-doping of $Na_3V_{2-x}Ti_x(PO_4)_2F_3$ compounds for sodium ion battery cathodes: Analysis of electrochemical performance and kinetic properties. *Nano Energy* **2018**, *47*, 340–352. [CrossRef]
38. Guo, J.Z.; Wang, P.F.; Wu, X.L.; Zhang, X.H.; Yan, Q.; Chen, H.; Zhang, J.P.; Guo, Y.G. High-Energy/Power and Low-Temperature Cathode for Sodium-Ion Batteries: In Situ XRD Study and Superior Full-Cell Performance. *Adv. Mater.* **2017**, *29*, 1701968. [CrossRef]
39. Xu, J.; Chen, J.; Tao, L.; Tian, Z.; Zhou, S.; Zhao, N.; Wong, C.-P. Investigation of $Na_3V_2(PO_4)_2O_2F$ as a sodium ion battery cathode material: Influences of morphology and voltage window. *Nano Energy* **2019**, *60*, 510–519. [CrossRef]
40. Park, Y.U.; Seo, D.H.; Kwon, H.S.; Kim, B.; Kim, J.; Kim, H.; Kim, I.; Yoo, H.I.; Kang, K. A new high-energy cathode for a Na-ion battery with ultrahigh stability. *J. Am. Chem. Soc.* **2013**, *135*, 13870–13878. [CrossRef]
41. Zhu, J.; Li, Y.; Yang, B.; Liu, L.; Li, J.; Yan, X.; He, D. A Dual Carbon-Based Potassium Dual Ion Battery with Robust Comprehensive Performance. *Small* **2018**, *14*, 1801836. [CrossRef]
42. Drozhzhin, O.A.; Tertov, I.V.; Alekseeva, A.M.; Aksyonov, D.A.; Stevenson, K.J.; Abakumov, A.M.; Antipov, E.V. β-$NaVP_2O_7$ as a Superior Electrode Material for Na-Ion Batteries. *Chem. Mater.* **2019**, *31*, 7463–7469. [CrossRef]
43. Kim, J.; Park, I.; Kim, H.; Park, K.-Y.; Park, Y.-U.; Kang, K. Tailoring a New 4V-Class Cathode Material for Na-Ion Batteries. *Adv. Energy Mater.* **2016**, *6*, 1502147. [CrossRef]
44. Kovrugin, V.M.; Chotard, J.-N.; Fauth, F.; Masquelier, C. $Na_7V_3(P_2O_7)_4$ as a high voltage electrode material for Na-ion batteries: Crystal structure and mechanism of Na+ extraction/insertion by operando X-ray diffraction. *J. Mater. Chem. A* **2020**, *8*, 21110–21121. [CrossRef]
45. Barpanda, P.; Liu, G.; Avdeev, M.; Yamada, A. t-$Na_2(VO)P_2O_7$: A 3.8 V Pyrophosphate Insertion Material for Sodium-Ion Batteries. *ChemElectroChem* **2014**, *1*, 1488–1491. [CrossRef]
46. Tang, L.; Zhang, J.; Li, Z.; Liu, X.; Xu, Q.; Liu, H.; Wang, Y.; Xia, Y.; Ma, Z. Using $Na_7V_4(P_2O_7)_4(PO_4)$ with superior Na storage performance as bipolar electrodes to build a novel high-energy-density symmetric sodium-ion full battery. *J. Power Sources* **2020**, *451*, 227734. [CrossRef]
47. Fang, W.; An, Z.; Xu, J.; Zhao, H.; Zhang, J. Superior performance of $Na_7V_4(P_2O_7)_4PO_4$ in sodium ion batteries. *RSC Adv.* **2018**, *8*, 21224–21228. [CrossRef]
48. Li, H.; Guan, C.; Xu, M.; Guo, J.; Yuan, K.; Cheng, K.; Xie, Y.; Zhang, L.; Zheng, J.; Lai, Y.; et al. Organic/inorganic anions coupling enabled reversible high-valent redox in vanadium-based polyanionic compound. *Energy Storage Mater.* **2022**, *47*, 526–533. [CrossRef]
49. Bui, K.M.; Dinh, V.A.; Okada, S.; Ohno, T. Na-ion diffusion in a NASICON-type solid electrolyte: A density functional study. *Phys. Chem. Chem. Phys.* **2016**, *18*, 27226–27231. [CrossRef]
50. Zhang, X.; Rui, X.; Chen, D.; Tan, H.; Yang, D.; Huang, S.; Yu, Y. $Na_3V_2(PO_4)_3$: An advanced cathode for sodium-ion batteries. *Nanoscale* **2019**, *11*, 2556–2576. [CrossRef]
51. Saravanan, K.; Mason, C.W.; Rudola, A.; Wong, K.H.; Balaya, P. The First Report on Excellent Cycling Stability and Superior Rate Capability of $Na_3V_2(PO_4)_3$ for Sodium Ion Batteries. *Adv. Energy Mater.* **2013**, *3*, 444–450. [CrossRef]
52. Jian, Z.; Han, W.; Lu, X.; Yang, H.; Hu, Y.-S.; Zhou, J.; Zhou, Z.; Li, J.; Chen, W.; Chen, D.; et al. Superior Electrochemical Performance and Storage Mechanism of $Na_3V_2(PO_4)_3$ Cathode for Room-Temperature Sodium-Ion Batteries. *Adv. Energy Mater.* **2013**, *3*, 156–160. [CrossRef]
53. Jian, Z.; Yuan, C.; Han, W.; Lu, X.; Gu, L.; Xi, X.; Hu, Y.-S.; Li, H.; Chen, W.; Chen, D.; et al. Atomic Structure and Kinetics of NASICON $Na_xV_2(PO_4)_3$ Cathode for Sodium-Ion Batteries. *Adv. Funct. Mater.* **2014**, *24*, 4265–4272. [CrossRef]
54. Bui, K.M.; Dinh, V.A.; Okada, S.; Ohno, T. Hybrid functional study of the NASICON-type $Na_3V_2(PO_4)_3$: Crystal and electronic structures, and polaron-Na vacancy complex diffusion. *Phys. Chem. Chem. Phys.* **2015**, *17*, 30433–30439. [CrossRef]
55. Jian, Z.; Zhao, L.; Pan, H.; Hu, Y.-S.; Li, H.; Chen, W.; Chen, L. Carbon coated $Na_3V_2(PO_4)_3$ as novel electrode material for sodium ion batteries. *Electrochem. Commun.* **2012**, *14*, 86–89. [CrossRef]
56. Shen, W.; Li, H.; Guo, Z.; Wang, C.; Li, Z.; Xu, Q.; Liu, H.; Wang, Y.; Xia, Y. Double-Nanocarbon Synergistically Modified $Na_3V_2(PO_4)_3$: An Advanced Cathode for High-Rate and Long-Life Sodium-Ion Batteries. *ACS Appl. Mater. Interfaces* **2016**, *8*, 15341–15351. [CrossRef]
57. Zakharkin, M.V.; Drozhzhin, O.A.; Ryazantsev, S.V.; Chernyshov, D.; Kirsanova, M.A.; Mikheev, I.V.; Pazhetnov, E.M.; Antipov, E.V.; Stevenson, K.J. Electrochemical properties and evolution of the phase transformation behavior in the NASICON-type $Na_{3+x}Mn_xV_{2-x}(PO_4)_3$ ($0 \leq x \leq 1$) cathodes for Na-ion batteries. *J. Power Sources* **2020**, *470*, 228231. [CrossRef]
58. Chen, Y.; Xu, Y.; Sun, X.; Zhang, B.; He, S.; Li, L.; Wang, C. Preventing structural degradation from $Na_3V_2(PO_4)_3$ to $V_2(PO_4)_3$: F-doped $Na_3V_2(PO_4)_3$/C cathode composite with stable lifetime for sodium ion batteries. *J. Power Sources* **2018**, *378*, 423–432. [CrossRef]
59. Nie, P.; Zhu, Y.; Shen, L.; Pang, G.; Xu, G.; Dong, S.; Dou, H.; Zhang, X. From biomolecule to $Na_3V_2(PO_4)_3$/nitrogen-decorated carbon hybrids: Highly reversible cathodes for sodium-ion batteries. *J. Mater. Chem. A* **2014**, *2*, 18606–18612. [CrossRef]
60. Guo, J.Z.; Wu, X.L.; Wan, F.; Wang, J.; Zhang, X.H.; Wang, R.S. A Superior $Na_3V_2(PO_4)_3$-Based Nanocomposite Enhanced by Both N-Doped Coating Carbon and Graphene as the Cathode for Sodium-Ion Batteries. *Chemistry* **2015**, *21*, 17371–17378. [CrossRef]
61. Jiang, Y.; Zhou, X.; Li, D.; Cheng, X.; Liu, F.; Yu, Y. Highly Reversible Na Storage in $Na_3V_2(PO_4)_3$ by Optimizing Nanostructure and Rational Surface Engineering. *Adv. Energy Mater.* **2018**, *8*, 1800068. [CrossRef]

62. Duan, W.; Zhu, Z.; Li, H.; Hu, Z.; Zhang, K.; Cheng, F.; Chen, J. $Na_3V_2(PO_4)_3$@C core–shell nanocomposites for rechargeable sodium-ion batteries. *J. Mater. Chem. A* **2014**, *2*, 8668–8675. [CrossRef]
63. Wang, Q.; Zhao, B.; Zhang, S.; Gao, X.; Deng, C. Superior sodium intercalation of honeycomb-structured hierarchical porous $Na_3V_2(PO_4)_3$/C microballs prepared by a facile one-pot synthesis. *J. Mater. Chem. A* **2015**, *3*, 7732–7740. [CrossRef]
64. Kovrugin, V.M.; David, R.; Chotard, J.N.; Recham, N.; Masquelier, C. A High Voltage Cathode Material for Sodium Batteries: $Na_3V(PO_4)_2$. *Inorg. Chem.* **2018**, *57*, 8760–8768. [CrossRef]
65. Hao, X.; Xie, H.; Zhang, X.; Wang, R.; Yu, S.; Liu, Y.; Yu, Y.; Xu, Y.; Sun, K. Electrochemical properties and sodium ion diffusion in $Na_3V(PO_4)_2$. *J. Solid State Chem.* **2020**, *281*, 121047. [CrossRef]
66. Kuganathan, N.; Chroneos, A. $Na_3V(PO_4)_2$ cathode material for Na ion batteries: Defects, dopants and Na diffusion. *Solid State Ion.* **2019**, *336*, 75–79. [CrossRef]
67. Liu, R.; Liang, Z.; Xiang, Y.; Zhao, W.; Liu, H.; Chen, Y.; An, K.; Yang, Y. Recognition of $V^{3+}/V^{4+}/V^{5+}$ Multielectron Reactions in $Na_3V(PO_4)_2$: A Potential High Energy Density Cathode for Sodium-Ion Batteries. *Molecules* **2020**, *25*, 1000. [CrossRef]
68. Boudin, S.; Guesdon, A.; Leclaire, A.; Borel, M.-M. Review on vanadium phosphates with mono and divalent metallic cations: Syntheses, structural relationships and classification, properties. *J Int. J. Inorg. Mater.* **2000**, *2*, 561–579. [CrossRef]
69. Dupré, N.; Wallez, G.; Gaubicher, J.; Quarton, M. Phase transition induced by lithium insertion in αI- and αII-$VOPO_4$. *J. Solid State Chem.* **2004**, *177*, 2896–2902. [CrossRef]
70. Zhu, Y.; Peng, L.; Chen, D.; Yu, G. Intercalation Pseudocapacitance in Ultrathin $VOPO_4$ Nanosheets: Toward High-Rate Alkali-Ion-Based Electrochemical Energy Storage. *Nano Lett.* **2016**, *16*, 742–747. [CrossRef]
71. Li, H.; Peng, L.; Zhu, Y.; Chen, D.; Zhang, X.; Yu, G. An advanced high-energy sodium ion full battery based on nanostructured $Na_2Ti_3O_7/VOPO_4$ layered materials. *Energy Environ. Sci.* **2016**, *9*, 3399–3405. [CrossRef]
72. Zhang, Z.; Ni, Y.; Avdeev, M.; Kan, W.H.; He, G. Dual-ion intercalation to enable high-capacity $VOPO_4$ cathodes for Na-ion batteries. *Electrochim. Acta* **2021**, *365*, 137376. [CrossRef]
73. Song, J.; Xu, M.; Wang, L.; Goodenough, J.B. Exploration of $NaVOPO_4$ as a cathode for a Na-ion battery. *Chem. Commun.* **2013**, *49*, 5280–5282. [CrossRef]
74. He, G.; Huq, A.; Kan, W.H.; Manthiram, A. β-$NaVOPO_4$ Obtained by a Low-Temperature Synthesis Process: A New 3.3 V Cathode for Sodium-Ion Batteries. *Chem. Mater.* **2016**, *28*, 1503–1512. [CrossRef]
75. Aparicio, P.A.; Dawson, J.A.; Islam, M.S.; de Leeuw, N.H. Computational Study of $NaVOPO_4$ Polymorphs as Cathode Materials for Na-Ion Batteries: Diffusion, Electronic Properties, and Cation-Doping Behavior. *J. Phys. Chem. C* **2018**, *122*, 25829–25836. [CrossRef]
76. Fang, Y.; Zhang, J.; Zhong, F.; Feng, X.; Chen, W.; Ai, X.; Yang, H.; Cao, Y. Amorphous $NaVOPO_4$ as a High-Rate and Ultrastable Cathode Material for Sodium-Ion Batteries. *CCS Chem.* **2021**, *3*, 2428–2436. [CrossRef]
77. Ding, J.; Lin, Y.C.; Liu, J.; Rana, J.; Zhang, H.; Zhou, H.; Chu, I.H.; Wiaderek, K.M.; Omenya, F.; Chernova, N.A.; et al. $KVOPO_4$: A New High Capacity Multielectron Na-Ion Battery Cathode. *Adv. Energy Mater.* **2018**, *8*, 1800221. [CrossRef]
78. Deriouche, W.; Anger, E.; Freire, M.; Maignan, A.; Amdouni, N.; Pralong, V. A vanadium oxy-phosphate $Na_4VO(PO_4)_2$ as cathode material for Na ion batteries. *Solid State Sci.* **2017**, *72*, 124–129. [CrossRef]
79. Ling, M.; Jiang, Q.; Li, T.; Wang, C.; Lv, Z.; Zhang, H.; Zheng, Q.; Li, X. The Mystery from Tetragonal $NaVPO_4F$ to Monoclinic $NaVPO_4F$: Crystal Presentation, Phase Conversion, and Na-Storage Kinetics. *Adv. Energy Mater.* **2021**, *11*, 2100627. [CrossRef]
80. Ling, M.; Lv, Z.; Li, F.; Zhao, J.; Zhang, H.; Hou, G.; Zheng, Q.; Li, X. Revisiting of Tetragonal $NaVPO_4F$: A High Energy Density Cathode for Sodium-Ion Batteries. *ACS Appl Mater Interfaces* **2020**, *12*, 30510–30519. [CrossRef]
81. Jin, T.; Liu, Y.; Li, Y.; Cao, K.; Wang, X.; Jiao, L. Electrospun $NaVPO_4F$/C Nanofibers as Self-Standing Cathode Material for Ultralong Cycle Life Na-Ion Batteries. *Adv. Energy Mater.* **2017**, *7*, 1700087. [CrossRef]
82. Zhao, J.; He, J.; Ding, X.; Zhou, J.; Ma Yo Wu, S.; Huang, R. A novel sol–gel synthesis route to $NaVPO_4F$ as cathode material for hybrid lithium ion batteries. *J. Power Sources* **2010**, *195*, 6854–6859. [CrossRef]
83. Zhao, C.-D.; Guo, J.-Z.; Gu, Z.-Y.; Zhao, X.-X.; Li, W.-H.; Yang, X.; Liang, H.-J.; Wu, X.-L. Robust three-dimensional carbon conductive network in a $NaVPO_4F$ cathode used for superior high-rate and ultralong-lifespan sodium-ion full batteries. *J. Mater. Chem. A* **2020**, *8*, 17454–17462. [CrossRef]
84. Kumar, V.K.; Ghosh, S.; Biswas, S.; Martha, S.K. Pitch-Derived Soft-Carbon-Wrapped $NaVPO_4F$ Composite as a Potential Cathode Material for Sodium-Ion Batteries. *ACS Appl. Energy Mater.* **2021**, *4*, 4059–4069. [CrossRef]
85. Zhang, X.; Zheng, F.; Lü, T.-Y.; Wu, S.; Zhu, Z. Probing the Limiting Mechanism of Sodium-Ion Extraction in the $Na_5V(PO_4)_2F_2$ Cathode. *J. Phys. Chem. C* **2021**, *125*, 14583–14589. [CrossRef]
86. Song, W.; Ji, X.; Wu, Z.; Yang, Y.; Zhou, Z.; Li, F.; Chen, Q.; Banks, C.E. Exploration of ion migration mechanism and diffusion capability for $Na_3V_2(PO_4)_2F_3$ cathode utilized in rechargeable sodium-ion batteries. *J. Power Sources* **2014**, *256*, 258–263. [CrossRef]
87. Nguyen, L.H.B.; Sanz Camacho, P.; Broux, T.; Olchowka, J.; Masquelier, C.; Croguennec, L.; Carlier, D. Density Functional Theory-Assisted ^{31}P and ^{23}Na Magic-Angle Spinning Nuclear Magnetic Resonance Study of the $Na_3V_2(PO_4)_2F_3$-$Na_3V_2(PO_4)_2FO_2$ Solid Solution: Unraveling Its Local and Electronic Structures. *Chem. Mater.* **2019**, *31*, 9759–9768. [CrossRef]
88. Xiong, H.; Liu, Y.; Shao, H.; Yang, Y. Understanding the electrochemical mechanism of high sodium selective material $Na_3V_2(PO_4)_2F_3$ in Li^+/Na^+ dual-ion batteries. *Electrochim. Acta* **2018**, *292*, 234–246. [CrossRef]

89. Guo, C.; Yang, J.; Cui, Z.; Qi, S.; Peng, Q.; Sun, W.; Lv, L.-P.; Xu, Y.; Wang, Y.; Chen, S. In-situ structural evolution analysis of Zr-doped $Na_3V_2(PO_4)_2F_3$ coated by N-doped carbon layer as high-performance cathode for sodium-ion batteries. *J. Energy Chem.* **2022**, *65*, 514–523. [CrossRef]
90. Gu, Z.-Y.; Guo, J.-Z.; Sun, Z.-H.; Zhao, X.-X.; Li, W.-H.; Yang, X.; Liang, H.-J.; Zhao, C.-D.; Wu, X.-L. Carbon-coating-increased working voltage and energy density towards an advanced $Na_3V_2(PO_4)_2F_3$@C cathode in sodium-ion batteries. *Sci. Bull.* **2020**, *65*, 702–710. [CrossRef]
91. Qi, Y.; Mu, L.; Zhao, J.; Hu, Y.-S.; Liu, H.; Dai, S. pH-regulative synthesis of $Na_3(VPO_4)_2F_3$ nanoflowers and their improved Na cycling stability. *J. Mater. Chem. A* **2016**, *4*, 7178–7184. [CrossRef]
92. Li, L.; Xu, Y.; Chang, R.; Wang, C.; He, S.; Ding, X. Unraveling the mechanism of optimal concentration for Fe substitution in $Na_3V_2(PO_4)_2F_3$/C for Sodium-Ion batteries. *Energy Storage Mater.* **2021**, *37*, 325–335. [CrossRef]
93. Liang, K.; Wang, S.; Zhao, H.; Huang, X.; Ren, Y.; He, Z.; Mao, J.; Zheng, J. A facile strategy for developing uniform hierarchical $Na_3V_2(PO_4)_2F_3$@carbonized polyacrylonitrile multi-clustered hollow microspheres for high-energy-density sodium-ion batteries. *Chem. Eng. J.* **2022**, *428*, 131780. [CrossRef]
94. Zhu, Y.; Xu, E.; Zhang, J.; Quan, J.; Wang, H.; Sun, Z.; Jiang, Y. Fabrication of a Sandwiched Core Carbon Sphere@$Na_3V_2(PO_4)_2O_2F$@N-Doped Carbon Cathode for Superior Sodium-Ion Batteries. *ACS Appl. Energy Mater.* **2021**, *4*, 3952–3961. [CrossRef]
95. Park, Y.-U.; Seo, D.-H.; Kim, H.; Kim, J.; Lee, S.; Kim, B.; Kang, K. A Family of High-Performance Cathode Materials for Na-ion Batteries, $Na_3(VO_{1-x}PO_4)_2F_{1+2x}(0 \leq x \leq 1)$: Combined First-Principles and Experimental Study. *Adv. Funct. Mater.* **2014**, *24*, 4603–4614. [CrossRef]
96. Fang, R.; Olchowka, J.; Pablos, C.; Bianchini Nuernberg, R.; Croguennec, L.; Cassaignon, S. Impact of the F^- for O^{2-} Substitution in $Na_3V_2(PO_4)_2F_{3-y}O_y$ on Their Transport Properties and Electrochemical Performance. *ACS Appl. Energy Mater.* **2022**, *5*, 1065–1075. [CrossRef]
97. Olchowka, J.; Nguyen, L.H.B.; Broux, T.; Sanz Camacho, P.; Petit, E.; Fauth, F.; Carlier, D.; Masquelier, C.; Croguennec, L. Aluminum substitution for vanadium in the $Na_3V_2(PO_4)_2F_3$ and $Na_3V_2(PO_4)_2FO_2$ type materials. *Chem. Commun. (Camb)* **2019**, *55*, 11719–11722. [CrossRef]
98. Nguyen, L.H.B.; Broux, T.; Camacho, P.S.; Denux, D.; Bourgeois, L.; Belin, S.; Iadecola, A.; Fauth, F.; Carlier, D.; Olchowka, J.; et al. Stability in water and electrochemical properties of the $Na_3V_2(PO_4)_2F_3$-$Na_3(VO)_2(PO_4)_2F$ solid solution. *Energy Storage Mater.* **2019**, *20*, 324–334. [CrossRef]
99. Nguyen, L.H.B.; Olchowka, J.; Belin, S.; Sanz Camacho, P.; Duttine, M.; Iadecola, A.; Fauth, F.; Carlier, D.; Masquelier, C.; Croguennec, L. Monitoring the Crystal Structure and the Electrochemical Properties of $Na_3(VO)_2(PO_4)_2F$ through Fe^{3+} Substitution. *ACS Appl. Mater. Interfaces* **2019**, *11*, 38808–38818. [CrossRef]
100. Serras, P.; Palomares, V.; Goñi, A.; Gil de Muro, I.; Kubiak, P.; Lezama, L.; Rojo, T. High voltage cathode materials for Na-ion batteries of general formula $Na_3V_2O_{2x}(PO_4)_2F_{3-2x}$. *J. Mater. Chem.* **2012**, *22*, 22301–22308. [CrossRef]
101. Serras, P.; Palomares, V.; Goñi, A.; Kubiak, P.; Rojo, T. Electrochemical performance of mixed valence $Na_3V_2O_{2x}(PO_4)_2F_{3-2x}$/C as cathode for sodium-ion batteries. *J. Power Sources* **2013**, *241*, 56–60. [CrossRef]
102. Sharma, N.; Serras, P.; Palomares, V.; Brand, H.E.A.; Alonso, J.; Kubiak, P.; Fdez-Gubieda, M.L.; Rojo, T. Sodium Distribution and Reaction Mechanisms of a $Na_3V_2O_2(PO_4)_2F$ Electrode during Use in a Sodium-Ion Battery. *Chem. Mater.* **2014**, *26*, 3391–3402. [CrossRef]
103. Mao, Z.; Wang, R.; He, B.; Gong, Y.; Wang, H. Large-Area, Uniform, Aligned Arrays of $Na_3(VO)_2(PO_4)_2F$ on Carbon Nanofiber for Quasi-Solid-State Sodium-Ion Hybrid Capacitors. *Small* **2019**, *15*, 1902466. [CrossRef] [PubMed]
104. Olchowka, J.; Fang, R.; Bianchini Nuernberg, R.; Pablos, C.; Carlier, D.; Cassaignon, S.; Croguennec, L. Particle nanosizing and coating with an ionic liquid: Two routes to improve the transport properties of $Na_3V_2(PO_4)_2FO_2$. *Nanoscale* **2022**, *14*, 8663–8676. [CrossRef]
105. Palomares, V.; Iturrondobeitia, A.; Sanchez-Fontecoba, P.; Goonetilleke, D.; Sharma, N.; Lezama, L.; Rojo, T. Iron-Doped Sodium–Vanadium Fluorophosphates: $Na_3V_{2-y}O_{2-y}Fe_y(PO_4)_2F_{1+y}$ (y < 0.3). *Inorg. Chem.* **2019**, *59*, 854–862.
106. Li, C.; Shen, M.; Lou, X.; Hu, B. Unraveling the Redox Couples of V^{III}/V^{IV} Mixed-Valent $Na_3V_2(PO_4)_2O_{1.6}F_{1.4}$ Cathode by Parallel-Mode EPR and In Situ/Ex Situ NMR. *J. Phys. Chem. C* **2018**, *122*, 27224–27232. [CrossRef]
107. Li, C.; Shen, M.; Hu, B.; Lou, X.; Zhang, X.; Tong, W.; Hu, B. High-energy nanostructured $Na_3V_2(PO_4)_2O_{1.6}F_{1.4}$ cathodes for sodium-ion batteries and a new insight into their redox chemistry. *J. Mater. Chem. A* **2018**, *6*, 8340–8348. [CrossRef]
108. Kee, Y.; Dimov, N.; Staikov, A.; Barpanda, P.; Lu, Y.-C.; Minami, K.; Okada, S. Insight into the limited electrochemical activity of $NaVP_2O_7$. *RSC Adv.* **2015**, *5*, 64991–64996. [CrossRef]
109. Vellaisamy, M.; Reddy, M.V.; Chowdari, B.V.R.; Kalaiselvi, N. Exploration of AVP_2O_7/C (A = Li, $Li_{0.5}Na_{0.5}$, and Na) for High-Rate Sodium-Ion Battery Applications. *J. Phys. Chem. C* **2018**, *122*, 24609–24618. [CrossRef]
110. Deng, C.; Zhang, S.; Zhao, B. First exploration of ultrafine $Na_7V_3(P_2O_7)_4$ as a high-potential cathode material for sodium-ion battery. *Energy Storage Mater.* **2016**, *4*, 71–78. [CrossRef]
111. Daidouh, A.; Veiga, M.; Pico, C. New polymorphs of $A_2VP_2O_8$ (A=Na, Rb): Structure determination and ionic conductivity. *Solid State Ion.* **1998**, *106*, 103–112. [CrossRef]
112. Lim, S.Y.; Kim, H.; Chung, J.; Lee, J.H.; Kim, B.G.; Choi, J.J.; Chung, K.Y.; Cho, W.; Kim, S.J.; Goddard, W.A., 3rd; et al. Role of intermediate phase for stable cycling of $Na_7V_4(P_2O_7)_4PO_4$ in sodium ion battery. *Proc. Natl. Acad. Sci. USA* **2014**, *111*, 599–604. [CrossRef] [PubMed]

113. Deng, C.; Zhang, S.; Wu, Y. Hydrothermal-assisted synthesis of the $Na_7V_4(P_2O_7)_4(PO_4)$/C nanorod and its fast sodium intercalation chemistry in aqueous rechargeable sodium batteries. *Nanoscale* **2015**, *7*, 487–491. [CrossRef] [PubMed]
114. Zhang, S.; Deng, C.; Meng, Y. Bicontinuous hierarchical $Na_7V_4(P_2O_7)_4(PO_4)$/C nanorod-graphene composite with enhanced fast sodium and lithium ions intercalation chemistry. *J. Mater. Chem. A* **2014**, *2*, 20538–20544. [CrossRef]
115. Deng, C.; Zhang, S. 1D nanostructured $Na_7V_4(P_2O_7)_4(PO_4)$ as high-potential and superior-performance cathode material for sodium-ion batteries. *ACS Appl. Mater. Interfaces* **2014**, *6*, 9111–9117. [CrossRef]
116. Li, Q.; Lin, B.; Zhang, S.; Deng, C. Towards high potential and ultra long-life cathodes for sodium ion batteries: Freestanding 3D hybrid foams of $Na_7V_4(P_2O_7)_4(PO_4)$ and $Na_7V_3(P_2O_7)_4$@biomass-derived porous carbon. *J. Mater. Chem. A* **2016**, *4*, 5719–5729. [CrossRef]
117. Zhao, D.; Wang, C.; Ding, Y.; Ding, M.; Cao, Y.; Chen, Z. Will Vanadium-Based Electrode Materials Become the Future Choice for Metal-Ion Batteries? *ChemSusChem* **2022**, *15*, e202200479. [CrossRef]